

Extended H₂ emission line sources from UWISH2

D. Froebrich^{1*}, S.V. Makin¹, C.J. Davis^{2,3}, T.M. Gledhill⁴, Y. Kim⁵, B.-C. Koo⁵, J. Rowles¹, J. Eisloffel⁶, J. Nicholas¹, J.J. Lee⁷, J. Williamson¹ A.S.M. Buckner¹

¹Centre for Astrophysics & Planetary Science, The University of Kent, Canterbury, Kent CT2 7NH, UK

²Division of Astronomical Sciences, National Science Foundation, 4201 Wilson Boulevard, Arlington, VA 22230, USA

³Astrophysics Research Institute, Liverpool John Moores University, Liverpool L3 5RF, UK

⁴Centre for Astrophysics Research, University of Hertfordshire, College Lane, Hatfield AL10 9AB, UK

⁵Department of Physics and Astronomy, Seoul National University, Seoul 151-747, Korea

⁶Thüringer Landessternwarte, Sternwarte 5, 07778 Tautenburg, Germany

⁷Korea Astronomy and Space Science Institute, Daejeon 305-348, Korea

Accepted. Received.

ABSTRACT

We present the extended source catalogue for the UKIRT Widefield Infrared Survey for H₂ (UWISH2). The survey is unbiased along the inner Galactic Plane from $l \approx 357^\circ$ to $l \approx 65^\circ$ and $|b| \leq 1.5^\circ$ and covers 209 square degrees. A further 42.0 and 35.5 square degrees of high dust column density regions have been targeted in Cygnus and Auriga. We have identified 33200 individual extended H₂ features. They have been classified to be associated with about 700 groups of jets and outflows, 284 individual (candidate) Planetary Nebulae, 30 Supernova Remnants and about 1300 Photo-Dissociation Regions. We find a clear decline of star formation activity (traced by H₂ emission from jets and photo-dissociation regions) with increasing distance from the Galactic Centre. About 60% of the detected candidate Planetary Nebulae have no known counterpart and 25% of all Supernova Remnants have detectable H₂ emission associated with them.

Key words: stars: formation – ISM: jets and outflows – ISM: planetary nebulae: general – ISM: supernova remnants – ISM: HII regions – ISM: individual: Galactic Plane

1 INTRODUCTION

The $\nu = 1 - 0$ (S1) ro-vibrational line of molecular hydrogen at $2.122 \mu\text{m}$ is particularly bright in warm, dense, molecular environments ($T \sim 2000 \text{ K}$, $n_{\text{H}} \geq 10^3 \text{ cm}^{-3}$). For this reason, this near-infrared line has been a much-used tracer of shocked molecular gas for a range of astrophysical phenomena, not least in outflows from the youngest protostars (e.g. Davis & Eisloffel (1995); Stanke et al. (2002); Davis et al. (2009); Varricatt et al. (2010); Ioannidis & Froebrich (2012a); Bally et al. (2014); Hartigan et al. (2015); Zhang et al. (2015); Wolf-Chase et al. (2015, in prep.)). H₂ may also be excited in photo-dissociation regions (PDRs) associated with young, intermediate-mass stars and HII regions (through fluorescence), as well as in post-AGB winds associated with Planetary and Proto-Planetary

Nebulae (PNe; in shocks or again via fluorescence) or in Supernova Remnants (SNRs).

In late 2006 we defined UWISH2, the UKIRT Wide Field Imaging Survey for H₂, as an unbiased, near-infrared, narrow-band imaging survey of the first Galactic quadrant. The region we initially targeted, covering an area between $10^\circ \leq l \leq 65^\circ$ and $-1.5^\circ \leq b \leq +1.5^\circ$, includes most of the giant molecular clouds and massive star forming regions in the northern hemisphere. Our goal with UWISH2 was to complement existing and proposed near-, mid- and far-infrared photometric surveys such as the Spitzer Space Telescope GLIMPSE survey (Benjamin et al. (2003); Churchwell et al. (2009)), the Galactic Plane Survey (GPS, Lucas et al. (2008)) of the UKIRT Infrared Deep Sky Survey (UKIDSS, Lawrence et al. (2007)), the James Clerk Maxwell Telescope Galactic Plane Survey (Moore et al. 2015, *subm.*), the Herschel Space Telescope Hi-Gal survey (Molinari et al. (2010)), by utilising the H₂ 1–0 S(1) line as a tracer of the

* E-mail: df@star.kent.ac.uk

dynamically active component of star formation (SF) not emphasised by the broad-band surveys.

Much of the UWISH2 survey area has also recently been imaged with the same telescope and instrument in narrow-band [FeII] line emission at $1.64\ \mu\text{m}$ (the UKIRT Wide Field Infrared Survey for Fe⁺ – UWIFE; Lee et al. (2014)). These observations are certainly complementary to the H₂ imaging presented here since [FeII] is an excellent tracer of the higher-excitation atomic gas in shocks and collimated jets (e.g. Nisini et al. (2002); Giannini et al. (2002); Giannini et al. (2004)).

The UWISH2 survey was completed in 2011 and is described in (Froebrich et al. 2011). An extension to the survey, referred to as UWISH2-E, was proposed in late 2012. Between December 2012 and December 2013, our large mosaic of H₂ images of the Galactic Plane (GP) was extended down through the Galactic Center to $l \sim 357^\circ$ (although this extension does not cover the full width of the original survey at all longitudes - see Sect. 2.2). We also partially mapped two new fields, one available in the summer, the other in winter, around the well-known high mass star forming regions in Cygnus and the more quiescent molecular cloud complex in Auriga.

In this paper we present the results of an unbiased search for all extended H₂ emission line features in the UWISH2 and UWISH2-E surveys. We aim to provide a comprehensive catalogue of extended 1–0S(1) features, their properties (position, size and flux) and most likely classification (as jet/outflow, PN, SNR or unclassified). This catalogue will be useful as a starting point for more detailed investigations of selected sub-sets of H₂ emission line objects, such as individual jets and outflows or PNe.

In Sect. 2 we describe the observations, survey areas, and data quality. In Sect. 3 we present the extended source catalogue and give a detailed account of the techniques used to find emission line features in the survey images. In Sect. 4 we discuss the overall properties of the detected H₂ emission line features, but refer to future publications for the detailed study of selected individual objects.

2 THE UWISH2 AND UWISH2-E SURVEYS

2.1 Observations

All data were acquired using the Wide Field Camera (WFCAM) on the United Kingdom Infrared Telescope (UKIRT), Mauna Kea, Hawaii. WFCAM houses four Rockwell Hawaii-II (HgCdTe 2048×2048 pixel) arrays spaced by 94% in the focal plane. The pixel scale measures $0''.4$, although micro-stepping is used to generate reduced mosaics with a $0''.2$ pixel scale and thereby fully sample the expected seeing.

For both the UWISH2 and UWISH2-E surveys we essentially repeated the observing strategy adopted by the UKIDSS GPS (Lucas et al. 2008), the only difference being the choice of filter and the exposure time used. Individual 60s exposures through a narrowband H₂ filter ($\lambda = 2.122\ \mu\text{m}$, $\delta\lambda = 0.021\ \mu\text{m}$) were repeated with a 2×2 point micro-stepping at three jitter positions. In this way 12 exposures were acquired at each telescope pointing, resulting in a total exposure time per pixel of 720s. Four telescope

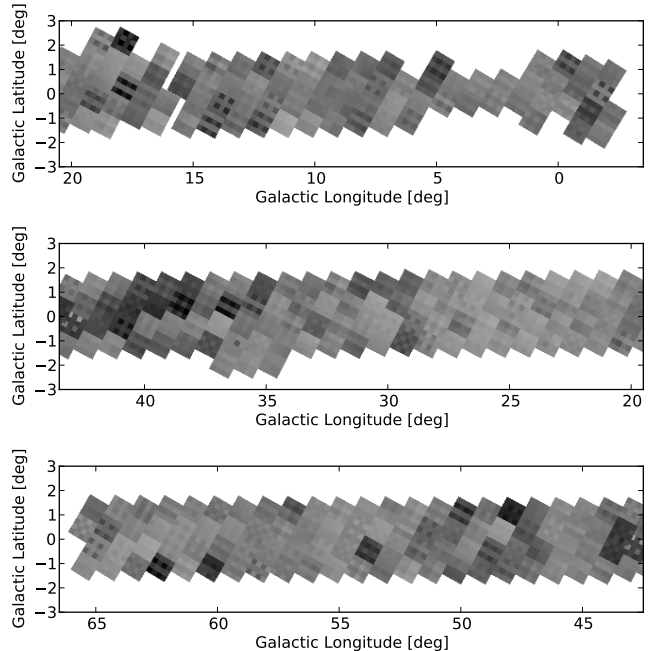


Figure 1. Plots of the seeing distribution in the Galactic Plane area of the survey. Positions covered by tiles/images with worse seeing are indicated by darker colours. See Sect. 2.3 for more details.

pointings are needed to fill in the gaps between the detectors; 16 mosaic images thus constitute a tile covering about 0.75 square degrees.

All data were reduced by the Cambridge Astronomical Survey Unit (CASU), which is responsible for data processing prior to archiving and distribution by the Wide Field Astronomy Unit (WFAU). The CASU reduction steps are described in detail by Dye et al. (2006); astrometric and photometric calibrations were achieved using 2MASS (Dye et al. (2006); Hewett et al. (2006)). The reduced images are available from WFAU as well as from the UWISH2 website¹, along with the corresponding broad-band J, H and K images from the GPS data. Continuum-subtracted H₂ –K images are also available, as are colour renditions of each 16-image tile.

2.2 Target Area

The survey covers the northern GP as well as selected high dust column density regions in Cygnus and Auriga. Along the GP we covered a longitude range from $l \approx 357^\circ$ to about $l \approx 65^\circ$. For most of this longitude range the survey covers the region $|b| \leq 1.5^\circ$. There are some extensions towards the North at $l \approx 19^\circ$ and towards the South at $l \approx 36^\circ$. Furthermore, due to time constraints we were unable to complete the full latitude range near the Galactic Centre. Figures 1 and 2 show the detailed coverage along the GP and in Cygnus and Auriga. In total we have observed 268 tiles with coverage in H₂ and the UKIDSS GPS K-band. Note

¹ Data available from <http://astro.kent.ac.uk/uwish2/>

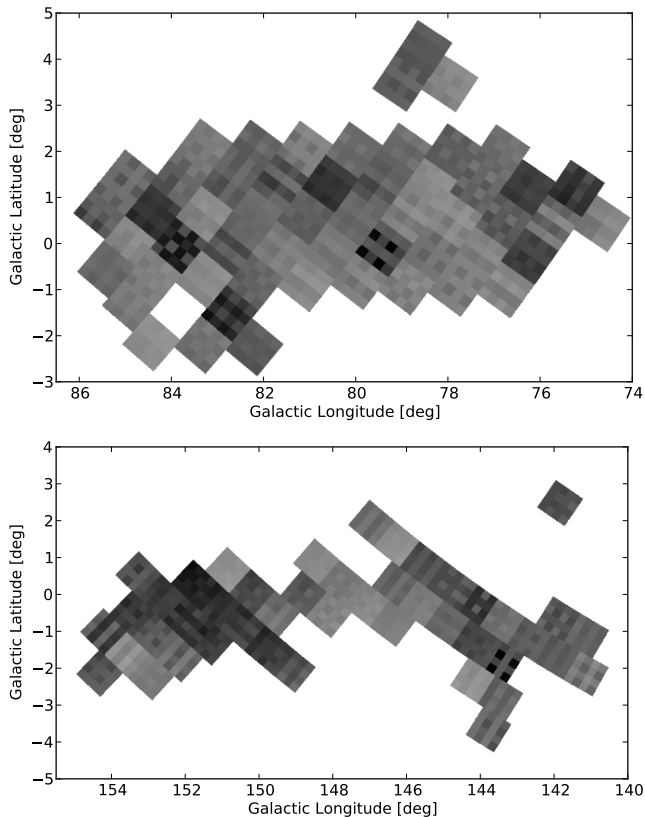


Figure 2. As Fig.1 but for the Cygnus (top) and Auriga (bottom) area of the survey.

that we have observed one additional tile just South of the Galactic Centre, but there is no K-band counterpart in the GPS database. We have searched the image for H_2 emission, but no features were detected.

Considering the overlap between images and tiles, the total area covered along the GP is 209 square degrees. In the Cygnus and Auriga areas the fields are roughly concentrated along the GP, but preference has been given to high extinction regions. Full coverage of the entire cloud complex could not be obtained due to time constraints. We have observed 54 tiles in Cygnus and 45 tiles in Auriga. Considering the overlap of images, this corresponds to 42.0 and 35.5 square degrees, respectively. Hence the total area covered in the entire UWISH2 survey is 286.5 square degrees.

Due to the nature of the observations, the coverage in both Galactic longitude and latitude in the survey area is not homogeneous. Hence any investigations of distributions of objects along and perpendicular to the GP will have to be corrected for the variations in relative coverage, i.e. a factor proportional to the number of images obtained at a specific latitude/longitude. In the top left panel of Fig.3 we show the relative coverage (normalised to a maximum of one) perpendicular to the GP. As can be seen, within 1.3° of the GP, the relative coverage exceeds 90% and is more or less homogeneous. Further away from the GP the coverage steeply declines and sinks below 10% at about 1.8° from the GP. A 50% coverage is achieved for all areas with $|b| < 1.5^\circ$. In the bottom left panel of Fig. 3 we show a similar

graph for the coverage along the GP. Between $l = 7^\circ$ and $l = 65^\circ$ the coverage is almost constant. Larger discrepancies are only seen near the GC and the two areas where we observed additional tiles slightly further away from the GP (at $l \approx 18^\circ$ and $l \approx 35^\circ$). For completeness, we also show the coverage distributions for the Cygnus and Auriga regions in the middle and right columns of Fig. 3, respectively. Due to the more patchy distribution of tiles in these clouds, the relative coverage in these cases is much more variable than along the GP.

2.3 Data Characteristics

The distribution of seeing values in our survey can be found in the left panel of Fig. 4. How these values are distributed spatially can be seen in Figs.1 and 2. The median seeing in the survey is $0''.79$, with 82.9% of the area observed at seeing values of below one arcsecond. Most of the poorer seeing data is distributed in the additional regions in Cygnus and Auriga. There, however, the crowding of stars is much less severe than in the inner GP, hence slightly worse seeing will not affect the detection and photometry of extended H_2 features.

We determine the background per pixel noise level in the images by estimating the *rms* scatter of the pixel values from the background, using a 3 sigma clipping procedure to remove stars. The counts are then converted into a surface brightness using the `mag_zp` values and integration times (for details see the calibration of photometry in Sect. 3.2). The distribution of the one pixel 1σ noise for all images is shown in the middle panel of Fig. 4. The median one pixel noise is $3.25 \times 10^{-19} \text{ W m}^{-2} \text{ arcsec}^{-2}$, in agreement with the typical noise in the original UWISH2 area (Froebrich et al. 2011). Averaged over the median seeing from above, which covers about 16 pixels, the typical 5σ noise or surface brightness detection limit is $4.1 \times 10^{-19} \text{ W m}^{-2} \text{ arcsec}^{-2}$. Alternatively, the 3σ noise over $1''.2$, the Glimpse pixel size, is $1.6 \times 10^{-19} \text{ W m}^{-2} \text{ arcsec}^{-2}$.

In the right panel of Fig. 4 we show the distribution of the photometric zero point values in the images. The narrow peak around 21.1 mag indicates that about two thirds of all images were taken under comparable atmospheric conditions, with extinction variations of less than 5%. This can also be seen in the Figs. A1 and A2 in the Appendix. We also summarise all the data for every image in the Appendix in Table C1. There we list the tile containing the image, the image name (containing the observation date), the centre of each image in RA, DEC (J2000) and l,b, the seeing, the calibration magnitude zero point and its uncertainty as well as the estimated one pixel surface brightness noise.

3 THE EXTENDED SOURCE CATALOGUE

In this section we describe the extended H_2 emission line object catalogue obtained from the UWISH2 images.

3.1 Source detection

To obtain an, as much as possible, complete and unbiased catalogue of extended H_2 emission line features, we performed the following steps for all images: i) Continuum

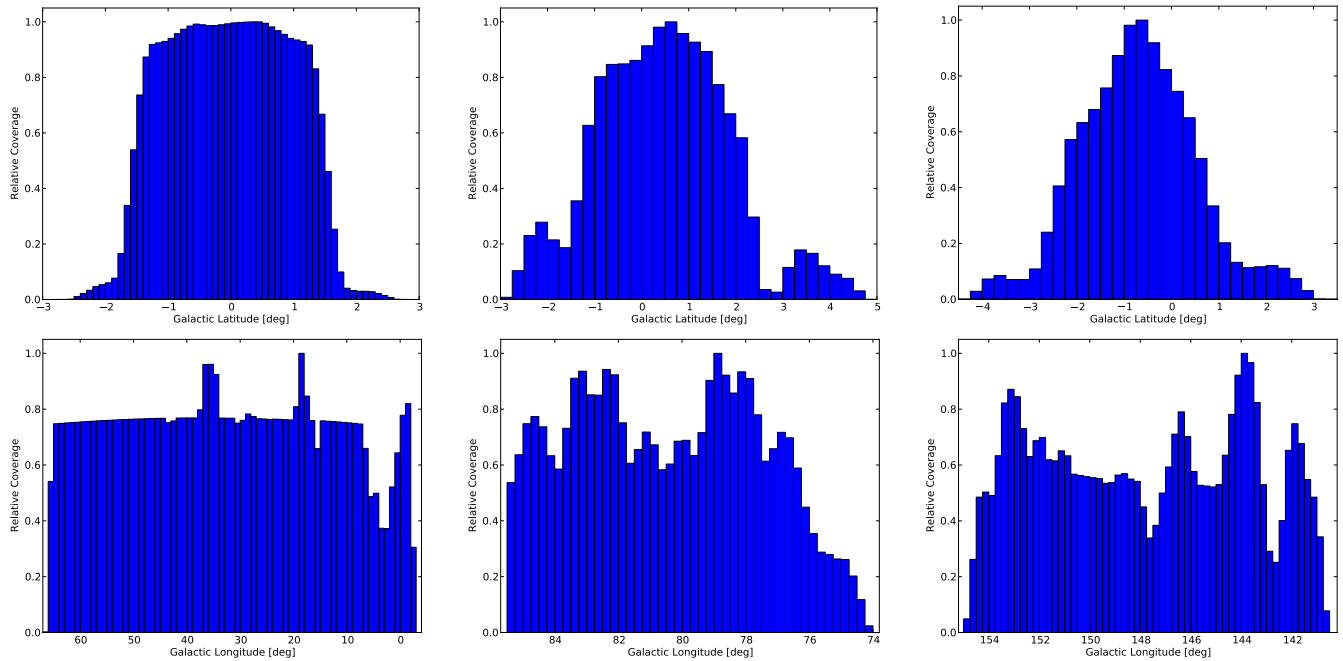


Figure 3. Relative latitude (top row) and longitude (bottom row) coverage of the survey in the Galactic Plane (left column), Cygnus (middle column) and Auriga (right column) area of the survey. The relative coverage is proportional to the number of images taken at a specific latitude/longitude and is normalised to a maximum of one. These distributions are used to correct observed distributions of objects such as Jets and PNe to account for the variations in coverage along and across the GP.

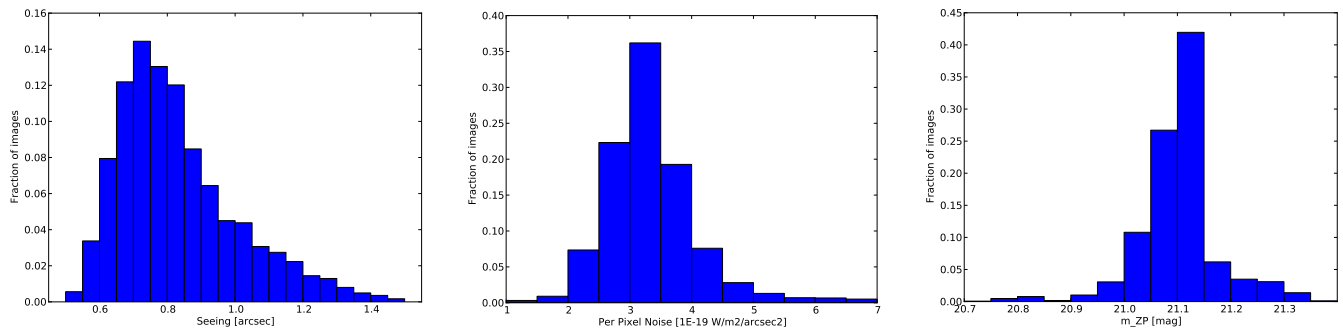


Figure 4. Data quality of the survey. The left panel shows the seeing distribution of our images, the middle panel shows the one sigma per pixel noise distribution and the right panel shows the distribution of the photometric zero point `mag_zp`. The median seeing is $0''.8$ and about 83% of the data has been taken with a seeing of less than one arcsecond. The median one sigma per pixel noise is $3.25 \times 10^{-19} \text{ W m}^{-2} \text{ arcsec}^{-2}$.

subtraction of the emission line images; ii) Filtering and automated detection of extended H_2 features; iii) Manual verification and removal of image artifacts. These steps are performed as described in detail below.

3.1.1 Continuum Subtraction

To remove the continuum emission from the H_2 narrow band images we utilised the K-band data from the UKIDSS GPS (Lucas et al. 2008). This continuum subtraction was done on an image by image basis, i.e. run separately for each $4\text{k} \times 4\text{k}$ image. Most of our H_2 images were taken at exactly the same positions as the GPS K-band data, with off-sets of less than a fraction of an arcminute. For a small fraction of fields, the off-sets were larger than one arcminute. In these cases we combined the K-band

images from the GPS to obtain a matching K-band image utilising the Montage² software. The image subtraction routine aligns the H_2 and K-band images, determines the scaling factor for the continuum image and uses psf-fitting to subtract the stars. The K-band scale factor and the psf shape are determined from unsaturated, isolated stars in $1000 \text{ pix} \times 1000 \text{ pix}$ sub-images. The details of the procedure are described in Lee et al. (2014). Note that the fluxes in the H_2 images are unchanged, and only the K-band continuum data are scaled.

These $\text{H}_2 - \text{K}$ difference images show many real H_2 emission line objects (such as shock excited Jets, SNRs or PNe), but also a large number of H_2 false positives caused by image and data analysis artifacts, as well as variability.

² <http://montage.ipac.caltech.edu/index.html>

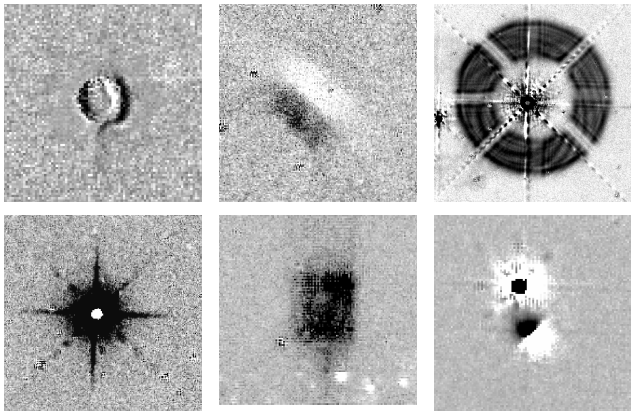


Figure 5. Example of false positives in the H₂ – K difference images. Suspected H₂ bright features are darker. From the top left to the bottom right, the panels show the following: i) electronic cross-talk from bright stars; ii) reflections from very bright stars; iii) diffraction rings around bright stars; iv) a variable (brighter during H₂ imaging) and saturated star; v) reflection from bright star just outside the edge (at bottom) of an image; vi) high proper motion star (next to variable star – fainter during H₂ imaging).

In Fig. 5 we show six examples of such potential false positives. Stars which are saturated or near the saturation limit (of about K=11 mag) are not subtracted completely. Furthermore, the K-band and H₂ images are typically taken several years apart from each other. Hence, any object that is variable, such as some giant stars or YSOs, might leave a positive or negative residual in the difference images, as do high proper motion stars. Furthermore, several kinds of image artifacts, such as reflections, memory effects from bright stars, and electronic cross-talk also leave residuals resembling H₂ emission line features. Finally, in cases where the two images had very different seeing, most stars were not removed completely.

3.1.2 Extended Source Detection

Most of the real H₂ features in our images are spatially resolved and have a low surface brightness. Furthermore, many of the extended features are projected onto a spatially variable background. Hence, before the detection of these extended, low surface brightness features, we filtered our images to remove remaining point sources and large scale variable background. We replace any small-scale structures (less than 2'' x 2'') that have a pixel value exceeding the 5 σ noise in the images with the local background. This will remove most un-subtracted point sources. We determined the *local* background as the median pixel value within 20'' and subtracted it from the H₂ – K difference images. Note that this will remove some of the largest scale features such as extended HII regions from the catalogue. However, in most cases a significant fraction of this emission will still be detected as several individual, smaller features. Hence in general we will have some detections of most extended objects. Readers interested in particular, very extended objects should however, re-process our H₂ – K difference images with an appropriate spatial filter.

We identified every region in the background subtracted

and point source removed images which was larger than four square arcseconds and had pixel values above half the *rms* noise in the images. This was done by plotting contours in ds9³ at the respective level. The shape of each closed contour is described by a polygon and is referred to as a '*region*' hereafter. The minimum size limit is essential to remove most of the remaining point sources and noise from the list of objects. We rejected every region that had a 2MASS point source within three arcseconds from the region centre to also automatically remove the majority of saturated stars from our list. Furthermore, many very bright stars (K < 7 mag) showed diffraction rings (e.g. top right panel in Fig. 5) that our procedure would pick up. We thus also removed every region that was completely within 35'' (slightly larger than the radius of the diffraction rings) from one of these very bright stars. Finally, all regions within 10'' from the edge of an image are removed. Note that the overlap between images is generally larger than this, hence no objects are lost in gaps. There is a small number of objects which have indeed multiple entries in the catalogue as they are detected (in whole or in part) on more than one image. We have not removed or joined these multiple entries in the final catalogue.

The requirements for the automated source detection (4 square arcseconds above the 0.5 σ single pixel noise level), combined with the 0''.2 x 0''.2 pixel size, can be used to estimate the detection limit. In essence the software will pick out any extended object whose surface brightness is higher than the 5 σ one pixel noise listed for every image. The one pixel noise values for all images are listed Table C1 in the Appendix.

3.1.3 Source verification/classification

The above automated detection procedure still included a large number of regions which were obviously not real H₂ features, and removed others which happened to be in the vicinity of bright stars. Hence, we manually checked all images to remove any region that was obviously not a real H₂ feature, e.g. image artifacts, variable or saturated stars and to re-add regions that were removed but clearly real. About 35% of all images were searched by two people independently to gain an understanding of the completeness and contamination of the selected H₂ features. The remaining images were only searched by one person. Based on the comparison of the catalogues obtained for the images with two people selecting objects as real, we estimate that the contamination of the catalogue with image artifacts or noise is very small. At most 1–2% of the catalogue entries might be artifacts. Also the completeness of the catalogues is very high. We estimate that more than 95% of all the real H₂ features detected automatically are in the final catalogue. Missing objects are usually small features in regions of large extended H₂ emission. These missing objects do not contribute with any significance to the total area or flux of the H₂ emission line catalogue.

During the above discussed manual verification of the automatically selected H₂ features, we also classified each feature into one of four categories: i) 'j' for all objects which

³ <http://ds9.si.edu/site/Home.html>

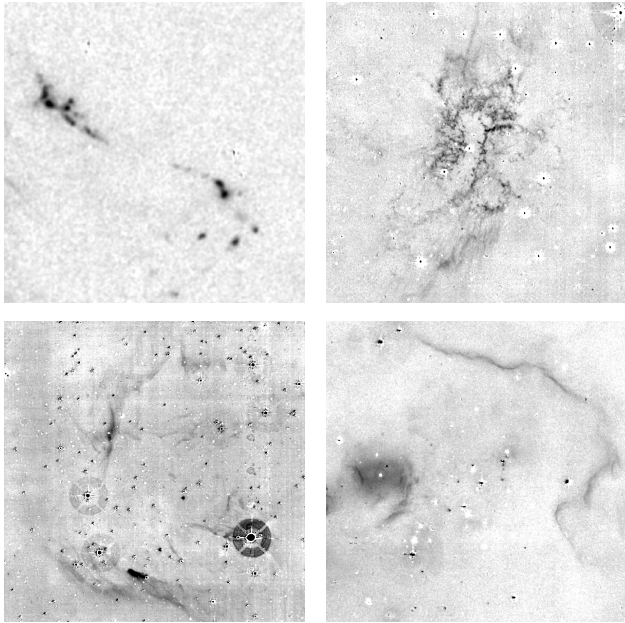


Figure 6. Example of real objects in the $H_2 - K$ difference images for each of our object categories. Suspected H_2 -bright features are darker. From the top left to the bottom right, the panels show the following: i) 'j' – outflow from IRAS 20294+4255; ii) 'p' – Planetary Nebula SH 2-71; iii) 's' – Supernova remnant G11.2-0.3; iv) 'u' – Emission near the cluster VDB 130.

seem to be part of a Jet or outflow from a young star. This classification was based on the shape of the feature, as well as its appearance/colour in the JKH_2 colour images. E.g. isolated, extended, high surface brightness H_2 knots which are situated in or near obvious star forming regions are classified as jet/outflow; ii) 'p' for objects that resemble known PNe. These tend to be ring-like, bipolar or in some cases more complex structures, typically not related to star forming regions. Note that in some cases the appearance alone is not sufficient to distinguish a bipolar PN from a Jet emanating from a young star. We furthermore checked the positions of all known PNe and candidates in the survey area and classified all H_2 features as 'p' if they were within a few arcsecond of a known object. We utilised the PNe entries in SIMBAD and the catalogues from IPHAS (Sabin et al. 2014), MASH (Parker et al. 2006) and MASH2 (Miszalski et al. 2008); iii) 's' for objects which are most likely part of a Galactic SNR. All H_2 features within the area of a known SNR (we utilised the list of Green (2009)) were selected to be of this category if they were not part of an obvious PN or Jet/outflow, or a small individual feature with no resemblance of the H_2 emission in other SNRs; iv) 'u' for all objects which could not be assigned to any of the other three categories. Note that the vast majority of these features are most likely part of PDRs surrounding HII regions. Thus, we refer to all the unclassified regions as PDRs. In Fig. 6 we show one example of each of the object categories.

Note that the source selection and classifications (except for the SNRs and the known PNe) were done blind, i.e. without using any catalogues of known objects or SIMBAD. This hence gives us a further estimate of

the completeness and accuracy of the classification by comparing to lists of known objects. We utilised the catalogue of Molecular Hydrogen emission line Objects (MHOs) from Ioannidis & Froebrich (2012a) who manually searched about 33 square degrees of early UWISH2 data for emission from jets and outflows. They list 134 MHOs and we have checked what fraction of these are contained in our catalogue: 83% of the MHOs are included in our extended- H_2 feature catalogue. Exclusively all of the non-detections (17%) are faint and small H_2 features which in most cases are similar to variable point sources rather than H_2 emission line objects. Of the detected H_2 features, 79% are also classified as being part of a jet or outflow, 15% are not classified ('u'), 4% coincide with emission from SNRs and 2% (2 MHOs) are listed as PN candidates in our list. Hence any objects missing in our catalogue are most likely faint and compact – indistinguishable from variable point sources.

3.2 Photometry

Flux measurement and calibration

Photometry has been obtained for each region in the $H_2 - K$ images. As these difference images are obtained by only scaling the K-band continuum fluxes, the H_2 flux in all the images is conserved. We identify all pixels inside each region and determine their median, maximum and total number of counts. We then correct these values by the local background counts. These are estimated as the median count value in a ring around each region with an inner radius equal to the radius of the region and an outer radius of twice this. Note that in some rare cases, this background estimate will be wrong, e.g. if a small region is situated close to a larger region of extended H_2 emission. These occurrences are rare, but might lead to background corrected fluxes which are erroneous or even negative. For a further discussion of uncertainties of the photometry see the end of this Section.

We convert the counts in each region into fluxes or surface brightness in two steps. Firstly the counts are converted into a magnitude via:

$$m = m_{zp} - 0.05 \cdot (X - 1) - 2.5 \cdot \log_{10} \left(\frac{\text{counts}}{t_{exp}} \right) - m_{ap} \quad (1)$$

where m_{zp} is the magnitude zero point for the observations, X the airmass during the observations, t_{exp} the exposure time in seconds and m_{ap} the aperture correction. As we are only considering extended sources we can set the aperture correction term to zero. All other terms are obtained from the FITS header in the H_2 images. Note that all our observations are taken with 720s integration time per pixel and the airmass is always between one and two. Hence, in most cases, the airmass term is of the same order or smaller than the uncertainty in m_{zp} . Furthermore, as can be seen in the right panel of Fig. 4, the general variations in m_{zp} are also only of the same order of magnitude. Note that m_{zp} includes the corrections that need to be made caused by the micro-stepping and hence $0''.2$ pixel size in our data.

These magnitudes are converted into fluxes by:

$$F = F_0^{H_2} \cdot 10^{-\frac{m}{2.5}} \quad (2)$$

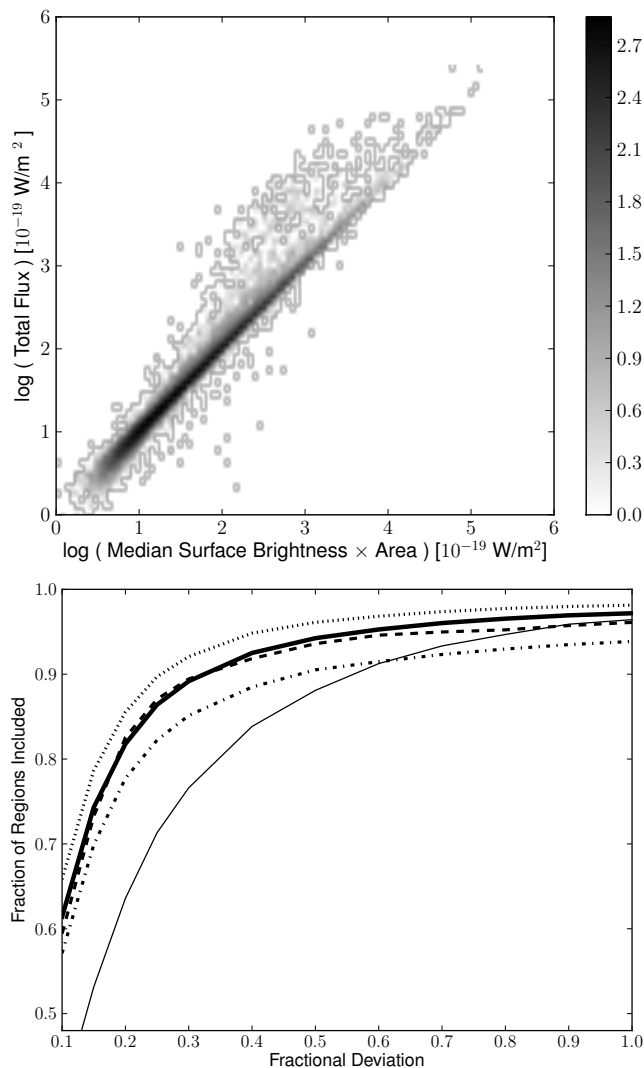


Figure 7. Top: Comparison of total flux and median surface brightness times area for all detected objects. The gray scale indicates the Log of the density of objects in each position. Most objects are very close to the 1:1 line. Bottom: Fractional deviation of the two flux estimates from the top panel vs. the fraction of objects which have a deviation smaller than it. The different line styles indicate the various objects: dot-dash line for SNRs, dashed line for PNe, bold solid line for all objects, dotted line for PDRs, thin solid line for jet features.

The m_{zp} values will calibrate the magnitudes into the 2MASS K-band. We thus used the 2MASS K-band flux zero point of $4.283 \cdot 10^{-10} \text{ W m}^{-2} \mu\text{m}^{-1}$ from Cohen et al. (2003) and the K-band filter width of $0.262 \mu\text{m}$ to determine the flux zero point $F_0^{H_2} = 1.12 \cdot 10^{-10} \text{ W m}^{-2}$. In combination the flux F corresponding to **counts** is determined as:

$$F = \text{counts} \cdot \frac{1.12 \cdot 10^{-10} \text{ W m}^{-2}}{t_{exp} [s]} \cdot 10^{\left\{ -\frac{m_{zp} - 0.05 \cdot (X-1)}{2.5} \right\}} \quad (3)$$

We compared our calibrated flux values to published flux values of jet knot and SNRs and they agree at the 10% level. Conversion of fluxes into surface brightness is done using the pixel size of 0.04 square arcseconds in our images.

Total flux estimates for objects

There are two ways to determine the entire H₂ flux of a region. We can: i) use the background corrected *total flux* inside a region (F_{tot}), or we can ii) multiply the background corrected median surface brightness by the area (or *median flux*) of the region (F_{med}). Both ways have obvious drawbacks. If the region contains a non-subtracted residual, either due to a saturation or variability (see also Fig. 5), then the total flux can be influenced (positively or negatively) by the presence of the star. If the median surface brightness is not a good estimate of the average H₂ flux, e.g. when a small fraction of the region contains a large fraction of the flux, the total flux will be underestimated. In order to compare the two methods we compare the estimated fluxes for both in the top panel of Fig. 7. It shows the density of objects, and in the majority of cases the two H₂ flux estimates are comparable. There are, however, a number of cases where the two estimates disagree by a large amount.

We investigate for what fraction of objects the two flux estimates agree within a given range. This is shown in the bottom panel of Fig. 7. The x-axis in the plot is the fractional deviation of the two fluxes (from 10% to a factor of two) and the y-axis shows the fraction of objects with a deviation smaller than this. The different line styles indicate the various object types. The bold solid line is for all objects, the thin solid line for jet features, the dotted line for PDRs, the dashed line for PNe and the dot-dash line for SNRs. As one can see from the figure, for about 80% of all objects the deviation of the two flux estimates is less than 20%. For the jet features the agreement is clearly worse, with only about 65% having flux estimates with a better than 20% agreement.

The reason for the latter seems to be the surface brightness distribution within jet knots. Most of them contain a small number of pixels which contribute a large fraction of the flux. This seems to be less an issue for PNe, PDRs and SNRs. We hence recommend to use F_{tot} for the total fluxes of all objects classified as jet, while for the other object types F_{med} seems more appropriate, as it prevents the potential inclusion of flux from (unsubtracted or variable) stars projected onto the H₂ emission line object. However, should the reader require more accurate photometry of selected objects, we recommend that they redo the flux estimate in our images, ensuring that only H₂ emitting areas are included in the photometry.

3.3 Object groups

Many of the detected H₂ emission features are not isolated, but are rather part of a group of objects. This is particularly true for the PNe and SNRs, which often consist of several emission features due to low surface brightness or large extent. We have hence grouped regions according to their spatial distribution. Objects were considered part of a group if they had a nearest neighbour within a given angular distance. For each group we determined properties such as the position, size (as the radius of a circle enclosing all group members) and total flux.

In the case of PNe regions, these groups can be considered as actual PN. We grouped objects automatically if they were separated by less than 3 arcminutes.

Additionally we inspected all of these PNe visually to ensure that there were no two PNe closer to each other than the 3' threshold and that the extended PNe in the catalogue had no 'outlying' features that were classified as a separate PN.

For the Jets and outflows it is not a simple task to identify which jet knots are part of which outflow and which object is the actual driving source of the jet. Such a procedure needs a detailed study of each region and is beyond the scope of this paper. However, groups of Jet/outflow knots can be considered as star forming regions with actively accreting YSOs. Given that a typical distance of jets and outflows in the survey area is about 3.5 kpc (Ioannidis & Froebrich 2012b) and the jets seem to occur in small groups of about 5 pc size (Ioannidis & Froebrich 2012a), we used 0.1 as minimum distance to separate groups of jets and outflows. Hence, these groups can be viewed as very young active star forming regions, slightly more extended than a typical young cluster (e.g. Schmeja et al. (2008)). Note that if moved to 3 kpc, the jets and outflows in NGC 1333 would be distributed over an area of about 2' x 2' on the sky.

The objects classified as 'u' (most likely HII regions or PDRs) are also grouped with the same minimum distance of 0.1, as they are probably at the same typical distances as the jet and outflow features. In essence these groups are likely to represent more evolved regions of star formation where the H₂ emission is caused by sources of ionising radiation.

We do not group the SNR objects in the same way as the other object types, since many of the SNRs are very extended on the sky. Instead, we have manually selected all the H₂ features which are part of each of the identified SNRs.

3.4 Catalogue description

The full extended H₂ feature catalogue displayed in Table D1 contains the following columns:

(i) Object ID; this is derived from the Galactic coordinates of the centre of each region. As centre we use the geometric centre of the polygon enclosing the detected H₂ emission.

(ii) Right Ascension and Declination (J2000) of the centre of the emission region.

(iii) Area A of the emission region in square arcseconds.

(iv) Radius r of the emission region in arcseconds; This is the minimum radius of a circle around the centre of the region that is enclosing all the emission.

(v) Median surface brightness F_{sb}^{med} of the region in $10^{-19} \text{ W m}^{-2} \text{ arcsec}^{-2}$; This is the surface brightness determined from the background corrected median intensity in the region.

(vi) Peak surface brightness F_{sb}^{max} of the region in $10^{-19} \text{ W m}^{-2} \text{ arcsec}^{-2}$; This is the peak surface brightness of the region. It might be influenced by the presence of stars inside the region.

(vii) One pixel *rms* noise surface brightness F_{σ} in $10^{-19} \text{ W m}^{-2} \text{ arcsec}^{-2}$; This is the one sigma *rms* of the background in a ring with inner radius r and outer radius $2r$ around each region (determined after sigma clipping to remove remaining stars and real emission features).

(viii) Total brightness F^{tot} of the region in $10^{-19} \text{ W m}^{-2}$;

This is the total flux measured in each region. It might be influenced by the presence of stars inside the region. An alternative measure of the total flux would be the product of the median surface brightness and area of the region.

(ix) Relative uncertainty $\Delta F/F$, in percent, of all fluxes due to the uncertainty in the magnitude zero point of the observations Δm_{zp} .

(x) Classification C of the object; This is a letter indicating what kind of object the region is most likely a part of. These are: j – jet or outflow from a YSO; p – part of a PN; s – part of a SNR; u – unknown nature, most likely part of a PDR near an HII region.

(xi) Name of the tile the region is on.

(xii) Name of the image the region is on.

(xiii) Group identifier the object belongs to. The group identifier contains the object type, as well as the Galactic coordinates of the group, calculated as the geometric centre of the features that make up the group.

4 RESULTS AND DISCUSSION

In this paper we will only discuss the general distribution and properties of the detected H₂ emission regions. For a detailed discussion of individual objects, or groups of objects we refer the reader to publications in preparation.

4.1 General Distributions

The entire survey region is composed of 5872 individual images. In only about one third of them (1935) have we identified real H₂ emission line features. This indicates that most areas, especially along the GP, are devoid of detectable H₂ emission, and that the detected H₂ features are localised/clustered. In total we detected 33200 individual extended H₂ emission line features. About 62% of them are situated in fields along the GP (37% in the inner and 25% in the outer GP – separated at $l = 30^\circ$), about 36% are in the Cygnus area, and the remaining 2% are in Auriga. Detailed results for the identified groups of objects are outlined in Tables 1 and 2. In these tables we break down the numbers for each of the survey regions for the different object classes (Jets, PNe, SNRs, unclassified – most likely PDRs). Furthermore, we show the total area covered by each part of the survey. We list the number of PNe, SNRs, the number of Jet groups (actively accreting star forming regions) and groups of other H₂ emission features, as well as their total fluxes, median fluxes and projected object densities in the different parts of the survey.

In Fig. 8 we show the spatial distributions of all the groups of objects (Jets, PNe, unknown/PDR) as well as their flux distributions. The distributions along the GP show that the objects are distributed slightly differently. In particular they are not in agreement with a homogeneous distribution in our survey. The distribution indicates that there are slightly less PNe than expected for a homogeneous distribution at Galactic longitudes less than 20° – 30° . This is most likely due to the higher extinction in this direction which will lower our detection limit to smaller distances. This is further supported by Table 2 which indicates the number of PNe per unit area in the inner GP is about 10% lower than in the outer GP. A KS-test shows that

Table 1. Table showing the different parts of the survey used in the analysis and some of the accumulated properties of the objects identified in them. We list the survey area, the sum of the total fluxes for each of the four object types and the total number of identified groups of objects. Note that for PNe and SNRs a ‘group’ identifies individual objects, while for Jets and PDRs a group simply refers to a group of spatially related individual H₂ features. The numbers in brackets indicate the fraction (as percent, rounded to the nearest integer) of the total flux or numbers of the total in the entire survey. We separate inner and outer GP at $l = 30^\circ$ and list all values for both together in the additional row labeled ‘GP’.

| Region | Area [deg ² (%)] | F _{tot} ^{Jet} | F _{tot} ^{PDR} [10 ⁻¹⁴ W m ⁻²] (%) | F _{tot} ^{PN} | F _{tot} ^{SNR} | N ^{Jet} | N ^{PDR} [Number (%)] | N ^{PN} | N ^{SNR} |
|------------|--------------------------------|---------------------------------|---|--------------------------------|---------------------------------|------------------|----------------------------------|-----------------|------------------|
| Total | 286.45 | 10.6 | 49.6 | 7.67 | 46.1 | 711 | 1309 | 284 | 30 |
| GP | 209.00 (73) | 4.70 (44) | 30.3 (61) | 7.37 (96) | 46.1 (100) | 450 (63) | 925 (71) | 261 (92) | 30 (100) |
| GP (Inner) | 95.18 (33) | 2.83 (27) | 24.7 (50) | 5.73 (75) | 15.5 (34) | 253 (36) | 489 (37) | 112 (39) | 20 (67) |
| GP (Outer) | 113.79 (40) | 1.86 (18) | 5.58 (11) | 1.64 (21) | 30.6 (66) | 197 (28) | 436 (33) | 149 (52) | 10 (33) |
| Cygnus | 41.99 (15) | 5.73 (54) | 18.3 (37) | 0.24 (3) | — | 210 (30) | 353 (27) | 16 (6) | — |
| Auriga | 35.46 (12) | 0.12 (1) | 1.13 (2) | 0.055 (1) | — | 51 (7) | 31 (2) | 7 (2) | — |

Table 2. Table listing the density (G, in objects per square degree) of the groups of objects in the various parts of the survey. We also list the median total flux (\bar{F}_{tot} in 10⁻¹⁹ W m⁻²) for each kind of group of objects. Note that for PNe and SNRs a ‘group’ identifies individual objects, while for Jets and PDRs a group simply refers to a group of spatially related individual H₂ features. We separate inner and outer GP at $l = 30^\circ$ and list all values for both together in the additional row labeled ‘GP’.

| Region | G ^{Jet} | G ^{PDR} | G ^{PN} | G ^{SNR} | $\bar{F}_{\text{tot}}^{\text{Jet}}$ | $\bar{F}_{\text{tot}}^{\text{PDR}}$ | $\bar{F}_{\text{tot}}^{\text{PN}}$ | $\bar{F}_{\text{tot}}^{\text{SNR}}$ |
|------------|------------------|------------------------------|-----------------|------------------|-------------------------------------|--|------------------------------------|-------------------------------------|
| | | [objects deg ⁻²] | | | | [10 ⁻¹⁹ W m ⁻²] | | |
| Total | 2.48 | 4.57 | 0.99 | 0.10 | 193 | 149 | 441 | 7096 |
| GP | 2.15 | 4.43 | 1.25 | 0.14 | 207 | 137 | 453 | 7096 |
| GP (inner) | 2.66 | 5.14 | 1.18 | 0.21 | 298 | 228 | 570 | 4345 |
| GP (outer) | 1.73 | 3.83 | 1.31 | 0.09 | 160 | 86.1 | 366 | 18120 |
| Cygnus | 5.00 | 8.41 | 0.38 | — | 204 | 183 | 173 | — |
| Auriga | 1.44 | 0.87 | 0.20 | — | 74.5 | 203 | 376 | — |

the PN longitude distribution has a 96.1% chance of being drawn from a homogeneous distribution. The longitude distributions of the groups of Jets and unknown/PDR objects, both of them representing star forming regions, are clearly different. There is a clear overabundance of objects compared to a homogeneous distribution for longitudes of less than 30°. A KS-test shows that both distributions have a probability of only 1.4% (Jets) and 3.0% (unknown/PDR) to be drawn from a homogeneous sample. It is also evident that groups (of both Jets and unknown/PDR objects) within 30° of the GC are much brighter than the groups further away (see Table 2), indicating stronger star formation activity (traced in H₂) closer to the GC. Furthermore, the spatial distribution of the groups of Jets and PDRs is much more clustered than for the PNe. Hence, the small star forming groups follow the large scale filamentary structure of GMCs along the GP.

We also determined the scale height of the distribution of the objects perpendicular to the GP. We utilised the method developed by Buckner & Froebrich (2014) to obtain the scale height and zero point of a Galactic latitude distribution. For the PNe we find a scale height of $0^\circ.92 \pm 0^\circ.11$ with a zero point at $b = -0^\circ.01 \pm 0^\circ.01$. However, due to our limited latitude coverage, this scale height should be taken as a lower limit. Indeed there is a 38.9% KS-test probability that the distribution of PNe across the GP in our survey area is drawn from a homogeneously distributed

sample. The vertical zero point of the PN distribution coincides (within the uncertainties) with the GP. This shows that the PNe trace an older, evolved population of objects. For the Jets and PDRs the scale heights are smaller with $0^\circ.65 \pm 0^\circ.06$ and $0^\circ.66 \pm 0^\circ.04$, respectively. The distribution zero points are at $-0^\circ.18 \pm 0^\circ.01$ and $-0^\circ.17 \pm 0^\circ.01$, respectively. Thus, within the uncertainties, the scale height and zero points of these distributions are identical, even if a KS-test gives only a 34.1% probability that the vertical distributions of both groups are drawn from the same parent distribution. They hence trace the same component of the star formation process. The vertical zero points for groups of jets and unknown objects are significantly below the GP. This is in good agreement with them tracing active star formation, which coincides with the dust and young cluster distribution which is shifted below the GP in the longitude range of our survey (e.g. Drimmel et al. (2003), Marshall et al. (2006), Buckner & Froebrich (2014)).

4.2 Jets and Outflows, PDRs, Star Formation

We can use all the H₂ features which are classified as Jets or PDRs as indicators of star formation activity. Jets most commonly trace young, accreting protostars and/or Classical T-Tauri stars. Objects we have classified as PDRs

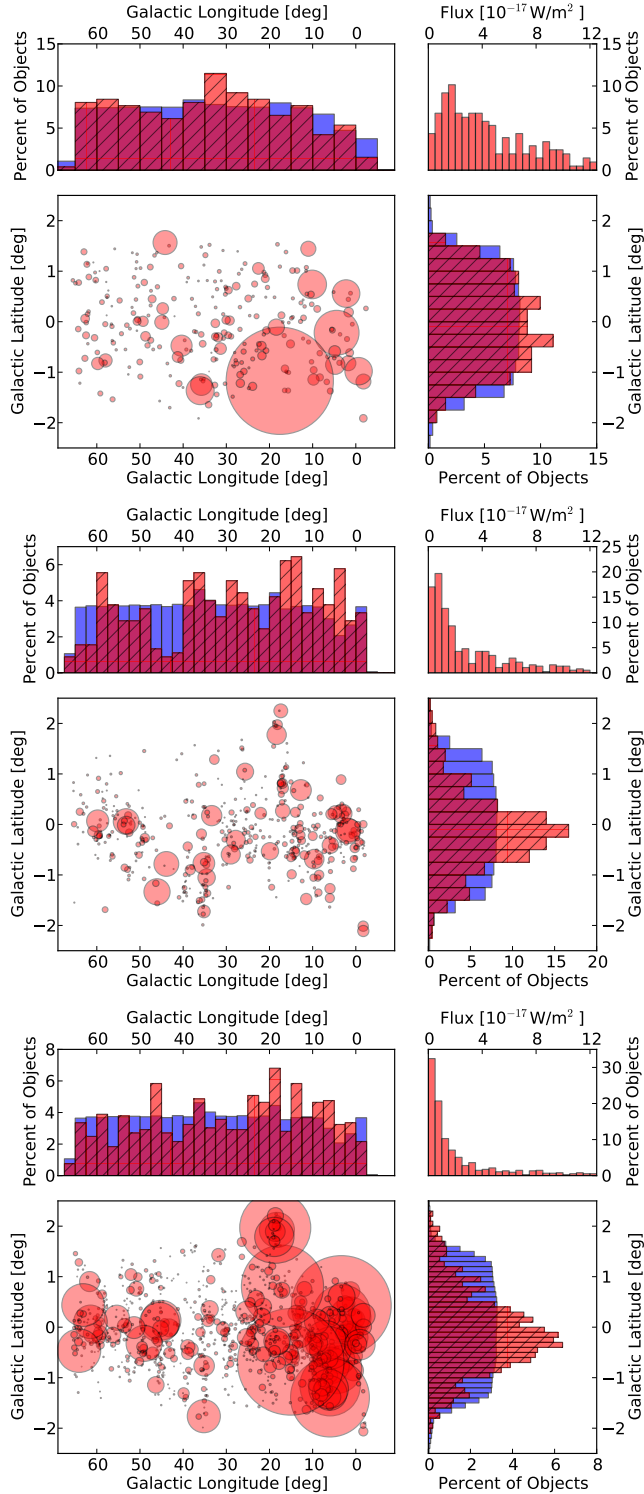


Figure 8. Distributions of PNe (top panel), jet groups (middle panel) and unknown objects (mostly PDRs, bottom panel). For each object type there are four plots. The bottom left indicates the spatial distribution where the circle size indicates the total flux of each group. The same scaling is applied in all plots. The top right graph show the distribution of the total fluxes for each group. Some of the bright groups of unknown objects are beyond the limit of the graph. The top left and bottom right graphs show the distribution of the number of objects along and across the GP (red, hatched) vs. the survey coverage (blue, unhatched).

are most likely excited by slightly more evolved young stars and are often found near clusters or intermediate mass stars.

Considering the respective survey areas, the Cygnus region clearly has the highest projected Jet/PDR group density. While along the GP there are on average about 2.15 Jet groups per square degree, in Cygnus the density is 5.00 per square degree. For PDRs there are 4.43 groups per square degree along the GP and 8.41 in Cygnus. This is most likely due to the fact that we specifically targeted high column density regions in Cygnus, i.e. active places of star formation. However, we used the same strategy in Auriga, which can be considered an example SF region in the outer GP, but we find on average only 1.44 Jet groups and 0.87 PDRs per square degree. This is a clear indication that the number of H_2 features is related to the general star formation activity which seems lowest in Auriga despite the bias in the survey. Furthermore, both SF indicators (Jets and PDRs) are clearly more prevalent in the inner GP compared to the outer GP.

A similar picture emerges if one uses the total flux of all features in each part of the survey to trace star formation activity. All the details are summarised in Table 1. The total H_2 flux per square degree from Jets is about 6.1 times higher in Cygnus compared to the GP. The flux per area for PDRs is 3.0 times higher in Cygnus than in the GP. In Auriga the flux per square degree from jets is 6.6 times lower than in the GP and for PDRs its 4.5 times lower. Thus, despite the focus on SF regions in the observations of Auriga, this region clearly stands out as the least active SF region in the survey.

We further investigate the median total fluxes for object groups, which we calculate by summing up the total fluxes of all H_2 features in the group and calculating the median over all groups (see Table 2). These fluxes can be considered as typical fluxes for each group of objects, as they are not influenced by extreme outliers (see e.g. the two extremely bright SNRs in Section 4.4). For Jet groups and PDRs these fluxes are generally lower in the outer GP than in the inner GP. For Jets the variations of the median total fluxes in the four sub-regions are less than a factor of a few, suggesting that the typical group of jets and outflows are similar in all the investigated regions and that extinction and distances to the typical Jet groups are comparable. Furthermore, the median total fluxes of the PDRs are very similar in the inner GP and Cygnus/Auriga, i.e. the typical SF regions in these areas are comparable in terms of their flux, but their numbers are highly variable.

In summary, the Jet and PDR features in the survey give a clear indication of the differences in the currently ongoing star formation activity (traced by H_2) in the areas covered by the survey. There are clearly more Jet groups and PDRs per unit area in the more active star forming regions but the individual objects are typically of a similar brightness. Please note that we cannot discuss any influences on the observed fluxes by systematic differences in distance and extinction to the typical objects observed in the various parts of the survey.

We are preparing more detailed investigations of the jets and outflows in Cygnus and Auriga. Several regions along the GP have also already been studied in detail (e.g. Ioannidis & Froebrich (2012a), Ioannidis & Froebrich (2012b), Froebrich & Ioannidis (2011), Lee et al. (2012),

Dewangan et al. (2012), Lim et al. (2012), Dewangan & Ojha (2013), Lee et al. (2013), Dewangan et al. (2015), Dewangan et al. (2015)).

4.3 Planetary Nebulae

A list of groups of H₂ detections which coincide with known PNe or which we consider to be new PNe candidates is given in Table B1 in the Appendix. We list the group/source ID (which contains the Galactic coordinates), Right Ascension and Declination, the radius of the circumscribing circle enclosing all detected H₂ emission, the area of emission, and the corresponding total and median fluxes. Finally, for previously known objects considered to be PNe, we give the PN G identifier where available. In cases where a known object is listed in SIMBAD but has not been identified as a PN then we give the alternative identifier (e.g. the IRAS name).

Approximately 60% of the H₂ detections in Table B1 correspond to emission features that have no corresponding source in SIMBAD and have not been identified as PN or PN candidates in the literature. We list these as *New* and have flagged them as possible PNe on the basis of their morphology and lack of association with known star formation activity. We stress that these are candidate PNe and their true nature will be established by follow-up observations (Gledhill et al. in prep.). These include two PNe candidates that have previously been identified as MHOs in (Ioannidis & Froebrich 2012a).

The number of PNe per square degree is 1.25 for the GP, with 1.18 and 1.31 per square degree in the inner and outer GP regions respectively (defined as $-3^\circ < l < 30^\circ$ and $30^\circ \leq l < 66^\circ$). Interestingly, the higher space density in the outer GP arises from *New* detections; 58% of H₂ detections in the inner GP are new, and 65% in the outer GP, corresponding to 0.68 and 0.85 objects per square degree, respectively. By contrast, the density of previously known PNe (with PN G identifiers) which also have H₂ emission, is 0.34 per square degree in both regions.

The lower space density of PNe in the inner GP may be a consequence of increased extinction along these sightlines. This is further supported by the larger median flux for inner GP PNe ($570 \times 10^{-19} \text{ W m}^{-2}$ compared with $366 \times 10^{-19} \text{ W m}^{-2}$) suggesting that we are sampling shorter sightlines. However, the higher fraction of *New* H₂-detected PNe in the outer, compared to inner GP (65% compared to 58%) indicates that we have not uncovered a population of inner-Galaxy PNe that were previously obscured in optical surveys. The Galactic distribution of H₂-detected PNe shown in Fig. 8 is actually similar to that of optically detected IPHAS PNe (Sabin et al. 2014).

4.4 Supernova Remnants

There are about 300 known SNRs in the Milky Way (Green 2014), and 119 SNRs are either fully or partially covered in the UWISH2 survey, including seven SNRs in Cygnus and one SNR in Auriga. We have detected H₂ emission features which are most likely associated with SNRs for 30 of them. Hence, the H₂ SNR detection rate is 25%. Table 3 lists the SNRs with H₂ emission features where we list the

SNR name, coordinates, sizes, types and other names. All parameters in this Table (except area covered in H₂ and fluxes) are from Green (2014). Please note that the SNR G6.5–0.4 also overlaps with several extended H₂ features. However, due to their visual appearance we attribute all of these to the larger, more extended SNR W 28.

The SNRs bright in H₂ emission in Table 3, e.g., W 28, 3C391, W 44, and W 49B, are prototypical SNRs interacting with molecular clouds. In these SNRs, the H₂ features fall on bright radio filaments, where the SN blast wave might be encountering dense environment. These H₂ emission features are probably shock excited. In some SNRs, however, H₂ features are just outside the radio continuum boundary (e.g. in G 11.2–0.3), and those features could be radiatively excited (Koo 2014). Note that W 44 and W 28 are responsible for 84% of the total H₂ emission associated with SNRs in our survey (57% and 27%, respectively). A much more detailed discussion of the H₂ emission features associated with SNRs will be presented in a forthcoming paper (Lee et al. 2015, in preparation).

5 CONCLUSIONS

We have used WFCAM at UKIRT to conduct a large survey for emission of the H₂ 1–0S(1) line at 2.122 μm . An unbiased survey along the GP from $l \approx 357^\circ$ to $l \approx 65^\circ$ and $|b| \leq 1.5^\circ$ covers about 209 square degrees. We have further targeted high column density areas in Cygnus (42.0 square degrees) and Auriga (35.5 square degrees).

We have compiled a catalogue of extended H₂ emission line features in this survey. All features were automatically detected and manually verified. We estimate that only 1–2% of the objects in the catalogue are false positives and that 95% of the real automatic detections are in the final catalogue. Mostly small features in the vicinity of larger extended H₂ emission might be missing but these do not contribute with any significance to the total detected H₂ flux. All features are also manually classified as either part of a Jet/outflow, PN or SNR. All other objects are unclassified but these are most likely part of PDRs.

In total, 33200 individual extended H₂ emission line features are contained in our catalogue. There are about 700 groups of jet/outflow features, 284 PNe, 30 SNRs and about 1300 groups of PDRs. The total H₂ flux is dominated by the PDR and SNR features (each accounting for 40–45% of all the flux). The Jet groups and PNe each contain about 7–9% of the flux.

We find that star formation (traced by H₂ emission of Jets and PDRs) is strongest in the inner GP (less than 30° from the Galactic Centre) and in the Cygnus region. The latter containing, due to our targeted survey, the highest number of Jet or PDR groups per square degree. Auriga clearly shows the lowest star formation activity based on all our measures (density of sources, total H₂ flux etc.) and there is also a clear decline in the star formation activity with distance from the Galactic Centre.

About 60% of all the PNe and candidate PNe in our catalogue have no known counterpart in any of the PNe catalogues. Hence our survey has uncovered a significant, unknown population of young and or embedded PNe

Table 3. List of SNRs with identified extended H₂ emission line features in our survey. The data (positions, size, type, 1 GHz flux, spectral index and other identifiers) are taken from Green (2014). The area covered by H₂ emission, the total and median fluxes as well as the number of individual H₂ emission regions are also listed. Note that G 6.5–0.4 also overlaps with several extended H₂ features. However, due to their visual appearance we attribute all of these to W 28.

| Name | RA (J2000) | DEC | Size [arcmin] | Area [arcmin ²] | 1 GHz flux [Jy] | spectral index | F _{tot} [10 ⁻¹⁵ W m ⁻²] | F _{med} | number of regions | type | other name |
|------------|---------------|--------|------------------|--------------------------------|--------------------|-------------------|--|------------------|----------------------|------|---------------|
| G1.0–0.1 | 17:48:30 | –28:09 | 8 | 0.12 | 15 | 0.6? | 0.24 | 0.22 | 4 | S | |
| G1.4–0.1 | 17:49:39 | –27:46 | 10 | 0.076 | 2? | ? | 0.43 | 0.18 | 7 | S | |
| G5.5+0.3 | 17:57:04 | –24:00 | 15x12 | 0.28 | 5.5 | 0.7 | 1.12 | 0.82 | 8 | S | |
| G6.1+0.5 | 17:57:29 | –23:25 | 18x12 | 0.052 | 4.5 | 0.9 | 0.11 | 0.10 | 3 | S | |
| G6.4–0.1 | 18:00:30 | –23:26 | 48 | 34.8 | 310 | varies | 126 | 89 | 1530 | C | W 28 |
| G9.9–0.8 | 18:10:41 | –20:43 | 12 | 0.11 | 6.7 | 0.4 | 0.10 | 0.09 | 20 | S | |
| G11.2–0.3 | 18:11:27 | –19:25 | 4 | 1.70 | 22 | 0.5 | 5.2 | 3.2 | 77 | C | |
| G13.5+0.2 | 18:14:14 | –17:12 | 5x4 | 0.049 | 3.5? | 1.0? | 0.06 | 0.05 | 6 | S | |
| G16.0–0.5 | 18:21:56 | –15:14 | 15x10 | 0.40 | 2.7 | 0.6 | 1.6 | 0.54 | 47 | S | |
| G18.1–0.1 | 18:24:34 | –13:11 | 8 | 0.34 | 4.6 | 0.5 | 3.0 | 0.92 | 48 | S | |
| G18.9–1.1 | 18:29:50 | –12:58 | 33 | 0.80 | 37 | 0.39 | 1.1 | 0.97 | 102 | C? | |
| G21.6–0.8 | 18:33:40 | –10:25 | 13 | 0.020 | 1.4 | 0.5? | 0.02 | 0.02 | 5 | S | |
| G21.8–0.6 | 18:32:45 | –10:08 | 20 | 1.75 | 65 | 0.56 | 4.3 | 3.7 | 119 | S | Kes 69 |
| G24.7+0.6 | 18:34:10 | –07:05 | 30x15 | 0.42 | 20? | 0.2? | 0.48 | 0.44 | 70 | C? | |
| G27.4+0.0 | 18:41:19 | –04:56 | 4 | 0.054 | 6 | 0.68 | 0.09 | 0.09 | 9 | S | 4C–04.71 |
| G27.8+0.6 | 18:39:50 | –04:24 | 50x30 | 0.11 | 30 | varies | 0.15 | 0.14 | 3 | F | |
| G28.8+1.5 | 18:39:00 | –02:55 | 100? | 0.046 | ? | 0.4? | 0.04 | 0.04 | 7 | S? | |
| G31.9+0.0 | 18:49:25 | –00:55 | 7x5 | 2.32 | 25 | varies | 15.6 | 7.2 | 102 | S | 3C391 |
| G32.1–0.9 | 18:53:10 | –01:08 | 40? | 0.55 | ? | ? | 1.8 | 0.70 | 71 | C? | |
| G32.8–0.1 | 18:51:25 | –00:08 | 17 | 2.20 | 11? | 0.2? | 7.5 | 2.9 | 203 | S? | Kes 78 |
| G33.2–0.6 | 18:53:50 | –00:02 | 18 | 0.12 | 3.5 | varies | 0.71 | 0.17 | 12 | S | |
| G34.7–0.4 | 18:56:00 | +01:22 | 35x27 | 62.9 | 250 | 0.37 | 263 | 157 | 2852 | C | W 44 |
| G38.7–1.3 | 19:06:40 | +04:28 | 32x19? | 0.26 | ? | ? | 0.57 | 0.29 | 43 | S | |
| G39.2–0.3 | 19:04:08 | +05:28 | 8x6 | 0.52 | 18 | 0.34 | 0.75 | 0.70 | 49 | C | 3C396 |
| G43.3–0.2 | 19:11:08 | +09:06 | 4x3 | 5.0 | 38 | 0.46 | 15.5 | 13.7 | 107 | S | W 49B |
| G54.4–0.3 | 19:33:20 | +18:56 | 40 | 0.39 | 28 | 0.5 | 0.52 | 0.41 | 54 | S | HC 40 |
| G65.1+0.6 | 19:54:40 | +28:35 | 90x50 | 0.13 | 5.5 | 0.61 | 0.06 | 0.09 | 7 | S | |
| G357.7+0.3 | 17:38:35 | –30:44 | 24 | 0.032 | 10 | 0.4? | 0.09 | 0.08 | 2 | S | |
| G359.0–0.9 | 17:46:50 | –30:16 | 23 | 0.15 | 23 | 0.5 | 0.30 | 0.30 | 10 | S | |
| G359.1–0.5 | 17:45:30 | –29:57 | 24 | 1.31 | 14 | 0.4? | 10.3 | 3.3 | 53 | S | |

candidates in the GP. Their spatial distribution, however, is very similar to the optically detected PNe.

Of all SNRs (partially) covered by our survey, one quarter has detectable H₂ emission. The total flux in these H₂ features is strongly dominated by W 44 and W 28 which together contain 84% of all the H₂ flux associated with SNRs.

ACKNOWLEDGEMENTS

The UWISH2 and UWISH2-E survey team would like to acknowledge the UKIRT support staff, particularly the Telescope System Specialists (Thor Wold, Tim Carroll and Jack Ehle) and the many UKIRT observers who have obtained data for the project via flexible scheduling. We would like to thank the Referee Paul Goldsmith for his helpful comments. We also acknowledge the Cambridge Astronomical Survey Unit and the WFCAM Science Archive for the reduction and ingest of the survey data. B.-C.K. was supported by the National Research Foundation of Korea (NRF) grant funded by the Korea Government (MSIP) (No.2012R1A4A1028713). The United Kingdom Infrared Telescope is operated by the Joint Astronomy Centre on behalf of the Science and Technology Facilities Council

of the U.K. Finally, we also thank the UKIRT Time Allocation Committee for their support of this long-term project. This research made use of Montage, funded by the National Aeronautics and Space Administration's Earth Science Technology Office, Computation Technologies Project, under Cooperative Agreement Number NCC5-626 between NASA and the California Institute of Technology. Montage is maintained by the NASA/IPAC Infrared Science Archive.

REFERENCES

- Bally J., Ginsburg A., Probst R., Reipurth B., Shirley Y. L., Stringfellow G. S., 2014, *Astronomical Journal*, 148, 120
- Benjamin R. A., Churchwell E., Babler B. L., Bania T. M., Clemens D. P., Cohen M., Dickey J. M., et al. 2003, *Publications of the ASP*, 115, 953
- Buckner A. S. M., Froebrich D., 2014, *Monthly Notices of the RAS*, 444, 290
- Churchwell E., Babler B. L., Meade M. R., Whitney B. A., Benjamin R., Indebetouw R., Cyganowski C., Robitaille T. P., Povich M., Watson C., Bracker S., 2009, *Publications of the ASP*, 121, 213

- Cohen M., Wheaton W. A., Megeath S. T., 2003, *Astronomical Journal*, 126, 1090
- Davis C. J., Eisloffel J., 1995, *Astronomy and Astrophysics*, 300, 851
- Davis C. J., Froebrich D., Stanke T., Megeath S. T., Kumar M. S. N., Adamson A., Eisloffel J., Gredel R., Khanzadyan T., Lucas P., Smith M. D., Varricatt W. P., 2009, *Astronomy and Astrophysics*, 496, 153
- Dewangan L. K., Mayya Y. D., Luna A., Ojha D. K., 2015, *Astrophysical Journal*, 803, 100
- Dewangan L. K., Ojha D. K., 2013, *Monthly Notices of the RAS*, 429, 1386
- Dewangan L. K., Ojha D. K., Anandarao B. G., Ghosh S. K., Chakraborti S., 2012, *Astrophysical Journal*, 756, 151
- Dewangan L. K., Ojha D. K., Grave J. M. C., Mallick K. K., 2015, *Monthly Notices of the RAS*, 446, 2640
- Drimmel R., Cabrera-Lavers A., López-Corredoira M., 2003, *Astronomy and Astrophysics*, 409, 205
- Dye S., Warren S. J., Hambly N. C., Cross N. J. G., Hodgkin S. T., Irwin M. J., Lawrence A., et al. 2006, *Monthly Notices of the RAS*, 372, 1227
- Froebrich D., Davis C. J., Ioannidis G., Gledhill T. M., Takami M., Chrysostomou A., Drew et al. 2011, *Monthly Notices of the RAS*, 413, 480
- Froebrich D., Ioannidis G., 2011, *Monthly Notices of the RAS*, 418, 1375
- Giannini T., McCoey C., Caratti o Garatti A., Nisini B., Lorenzetti D., Flower D. R., 2004, *Astronomy and Astrophysics*, 419, 999
- Giannini T., Nisini B., Caratti o Garatti A., Lorenzetti D., 2002, *Astrophysical Journal, Letters*, 570, L33
- Green D. A., 2009, *Bulletin of the Astronomical Society of India*, 37, 45
- Green D. A., 2014, *Bulletin of the Astronomical Society of India*, 42, 47
- Hartigan P., Reiter M., Smith N., Bally J., 2015, *Astronomical Journal*, 149, 101
- Hewett P. C., Warren S. J., Leggett S. K., Hodgkin S. T., 2006, *Monthly Notices of the RAS*, 367, 454
- Ioannidis G., Froebrich D., 2012a, *Monthly Notices of the RAS*, 421, 3257
- Ioannidis G., Froebrich D., 2012b, *Monthly Notices of the RAS*, 425, 1380
- Koo B.-C., 2014, in Ray A., McCray R. A., eds, *IAU Symposium Vol. 296 of IAU Symposium, Infrared [Fe II] and Dust Emissions from Supernova Remnants*. pp 214–221
- Lawrence A., Warren S. J., Almaini O., Edge A. C., Hambly N. C., Jameson R. F., Lucas P., et al. 2007, *Monthly Notices of the RAS*, 379, 1599
- Lee H.-T., Liao W.-T., Froebrich D., Karr J., Ioannidis G., Lee Y.-H., Su Y.-N., Liu S.-Y., Duan H.-Y., Takami M., 2013, *Astrophysical Journal, Supplement*, 208, 23
- Lee H.-T., Takami M., Duan H.-Y., Karr J., Su Y.-N., Liu S.-Y., Froebrich D., Yeh C. C., 2012, *Astrophysical Journal, Supplement*, 200, 2
- Lee J.-J., Koo B.-C., Lee Y.-H., Lee H.-G., Shinn J.-H., Kim H.-J., Kim Y., Pyo T.-S., Moon D.-S., Yoon S.-C., Chun M.-Y., Froebrich D., Davis C. J., Varricatt W. P., Kyeong J., Hwang N., Park B.-G., Lee M. G., Lee H. M., Ishiguro M., 2014, *Monthly Notices of the RAS*, 443, 2650
- Lim W., Lyo A.-R., Kim K.-T., Byun D.-Y., 2012, *Astronomical Journal*, 144, 151
- Lucas P. W., Hoare M. G., Longmore A., Schröder A. C., Davis C. J., Adamson A., Bandyopadhyay R. M., et al. 2008, *Monthly Notices of the RAS*, 391, 136
- Marshall D. J., Robin A. C., Reylé C., Schultheis M., Picaud S., 2006, *Astronomy and Astrophysics*, 453, 635
- Miszalski B., Parker Q. A., Acker A., Birkby J. L., Frew D. J., Kovacevic A., 2008, *Monthly Notices of the RAS*, 384, 525
- Molinari S., Swinyard B., Bally J., Barlow M., Bernard J.-P., Martin P., Moore T., et al. 2010, *Publications of the ASP*, 122, 314
- Nisini B., Caratti o Garatti A., Giannini T., Lorenzetti D., 2002, *Astronomy and Astrophysics*, 393, 1035
- Parker Q. A., Acker A., Frew D. J., Hartley M., Peyaud A. E. J., Ochsenbein F., Phillipps S., Russeil D., Beaulieu S. F., Cohen M., Köppen J., Miszalski B., Morgan D. H., Morris R. A. H., Pierce M. J., Vaughan A. E., 2006, *Monthly Notices of the RAS*, 373, 79
- Sabin L., Parker Q. A., Corradi R. L. M., Guzman-Ramirez L., Morris R. A. H., Zijlstra A. A., Bojičić I. S., et al. 2014, *Monthly Notices of the RAS*, 443, 3388
- Schmeja S., Kumar M. S. N., Ferreira B., 2008, *Monthly Notices of the RAS*, 389, 1209
- Stanke T., McCaughrean M. J., Zinnecker H., 2002, *Astronomy and Astrophysics*, 392, 239
- Varricatt W. P., Davis C. J., Ramsay S., Todd S. P., 2010, *Monthly Notices of the RAS*, 404, 661
- Zhang M., Fang M., Wang H., Sun J., Wang M., Jiang Z., Anathipindika S., 2015, *ArXiv e-prints*

APPENDIX A: MAP_ZP DISTRIBUTIONS

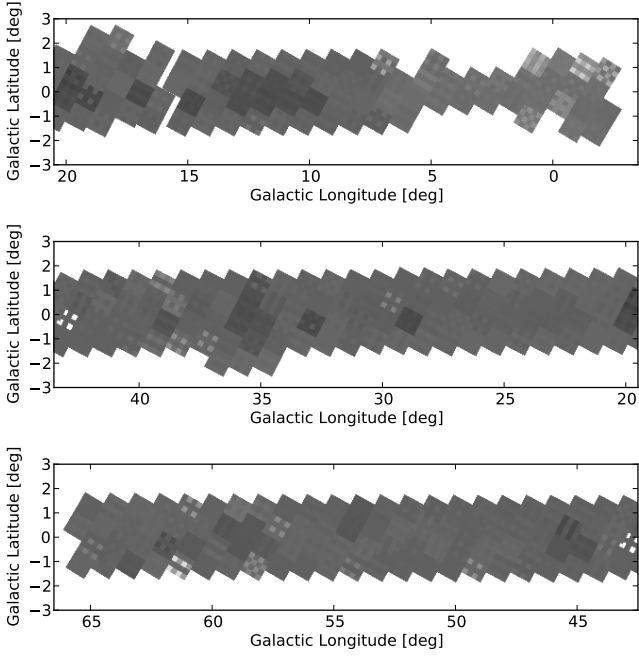


Figure A1. Plots and `mag_zp` distribution in the Galactic Plane area of the survey. Darker colours indicate higher values for `mag_zp`.

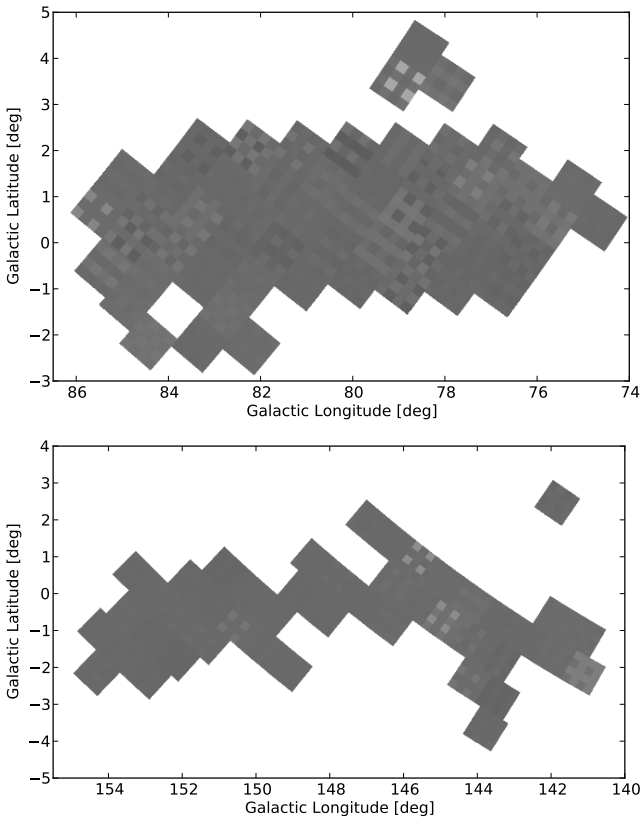


Figure A2. As Fig. A1 but for the Cygnus (top) and Auriga (bottom) area of the survey.

APPENDIX B: PROPERTIES OF PNE

Table B1: Table listing all the PNe detected in our survey. We list the UWISH2 PN source ID, which includes the Galactic coordinates, the RA and DEC (J2000) positions of the geometric centre of the H₂ emitting features in the PN, the radius around this central position enclosing all the H₂ emission, the area covered with H₂ emission, the total and median fluxes of the PN, and any other known name/identifier or coinciding object (not necessarily a PN). 'New' in the last column indicates objects that have so far not been recognised as PNe or PNe candidates in the literature.

| Source ID | RA [deg] | DEC [deg] | Radius [arcsec] | Area [arcsec ²] | F _{tot} [10 ⁻¹⁹ Wm ⁻²] | F _{med} | Other ID |
|-----------------------------|-------------|--------------|--------------------|--------------------------------|---|------------------|---------------------------|
| PN_UWISH2_000.81878-0.04944 | 266.93718 | -28.26207 | 6.3 | 52.97 | 388.50 | 345.89 | SSTGC 841071 |
| PN_UWISH2_001.22588+0.56414 | 266.58223 | -27.59584 | 5.7 | 44.18 | 386.74 | 331.79 | New |
| PN_UWISH2_001.42213-0.61357 | 267.83773 | -28.03457 | 16.9 | 243.11 | 1706.78 | 1796.58 | New |
| PN_UWISH2_001.65056+0.18803 | 267.19290 | -27.42713 | 14.8 | 298.48 | 2544.15 | 2286.36 | PN G001.6+00.1 |
| PN_UWISH2_001.72196-0.82262 | 268.21435 | -27.88315 | 17.3 | 211.92 | 6355.37 | 1543.66 | New |
| PN_UWISH2_001.73118+0.44232 | 266.99457 | -27.22684 | 12.2 | 137.19 | 498.93 | 439.01 | New |
| PN_UWISH2_002.03824-0.34363 | 267.93092 | -27.36701 | 23.4 | 149.54 | 680.57 | 655.32 | New |
| PN_UWISH2_002.25319+0.55724 | 267.18642 | -26.72043 | 47.7 | 1312.63 | 1712.21 | 9032.45 | PN G002.2+00.5 |
| PN_UWISH2_003.65197-0.25068 | 268.75783 | -25.92948 | 4.9 | 48.46 | 323.03 | 309.66 | New |
| PN_UWISH2_003.79367-0.81428 | 269.37918 | -26.09041 | 5.7 | 35.84 | 746.92 | 224.72 | New |
| PN_UWISH2_004.44847-0.21905 | 269.17220 | -25.22542 | 88.9 | 2267.66 | 7638.52 | 18397.78 | New |
| PN_UWISH2_004.76799-0.85257 | 269.95542 | -25.26527 | 17.1 | 289.48 | 0582.35 | 2023.47 | New |
| PN_UWISH2_004.88887-0.58981 | 269.77016 | -25.02963 | 38.6 | 690.14 | 3875.28 | 3181.93 | PN G004.8-00.5 |
| PN_UWISH2_004.99841-0.72107 | 269.95596 | -24.99999 | 6.5 | 60.86 | 338.48 | 306.73 | New |
| PN_UWISH2_005.14078+0.58616 | 268.79000 | -24.22186 | 6.5 | 40.10 | 205.82 | 202.82 | New |
| PN_UWISH2_005.42811-0.16852 | 269.66434 | -24.35213 | 26.1 | 178.42 | 906.42 | 848.62 | New |
| PN_UWISH2_005.56222-0.15023 | 269.72037 | -24.22679 | 10.5 | 112.38 | 478.75 | 485.48 | New |
| PN_UWISH2_005.90685-1.37325 | 271.07450 | -24.53226 | 17.8 | 279.37 | 992.38 | 1008.53 | New |
| PN_UWISH2_006.51856-0.69279 | 270.75465 | -23.66517 | 8.5 | 96.85 | 425.90 | 405.80 | New |
| PN_UWISH2_006.73073-1.19177 | 271.34313 | -23.72525 | 11.0 | 169.83 | 829.38 | 765.93 | New |
| PN_UWISH2_008.33574-1.10291 | 272.10781 | -22.28043 | 19.1 | 109.88 | 1414.41 | 551.62 | PN G008.3-01.1 |
| PN_UWISH2_008.36142-0.62384 | 271.66930 | -22.02504 | 8.9 | 112.93 | 794.42 | 606.43 | IRAS 18036-2201 |
| PN_UWISH2_008.94169+0.25318 | 271.15183 | -21.09003 | 15.7 | 205.01 | 1280.44 | 1158.31 | MGE G008.9409+00.2532 |
| PN_UWISH2_009.76150-0.95756 | 272.71231 | -20.96230 | 10.7 | 143.92 | 1308.31 | 761.34 | SSTGLMC G009.7612-00.9575 |
| PN_UWISH2_009.80708-1.14613 | 272.91283 | -21.01314 | 20.9 | 376.92 | 3534.44 | 3056.88 | PN G009.8-01.1 |
| PN_UWISH2_010.10373+0.73752 | 271.30883 | -19.83976 | 110.7 | 2993.26 | 23449.28 | 20473.46 | PN G010.1+00.7 |
| PN_UWISH2_010.21147+0.34469 | 271.72932 | -19.93758 | 30.7 | 190.12 | 571.03 | 555.52 | PN G010.2+00.3 |
| PN_UWISH2_010.26120-0.79452 | 272.81690 | -20.44591 | 8.0 | 132.78 | 537.11 | 512.53 | New |
| PN_UWISH2_010.39239+0.53966 | 271.64211 | -19.68458 | 20.1 | 301.02 | 1239.45 | 1159.96 | SSTGLMC G010.393+00.538 |
| PN_UWISH2_010.94194-0.40277 | 272.80040 | -19.66068 | 13.2 | 133.56 | 435.56 | 422.76 | New |
| PN_UWISH2_011.00185+1.44395 | 271.12230 | -18.71089 | 18.7 | 503.97 | 6480.38 | 3915.85 | PN G011.0+01.4 |
| PN_UWISH2_011.32982+0.54981 | 272.11575 | -18.86062 | 7.4 | 98.14 | 360.27 | 424.95 | New |
| PN_UWISH2_011.45829+1.07349 | 271.69860 | -18.49376 | 4.0 | 49.55 | 455.05 | 345.22 | IRAS 18038-1830 |
| PN_UWISH2_011.52915+1.00385 | 271.79911 | -18.46579 | 8.2 | 72.03 | 181.51 | 188.48 | PN G011.5+01.0 |
| PN_UWISH2_011.86338+0.30190 | 272.61733 | -18.51366 | 6.0 | 67.67 | 292.62 | 280.15 | New |
| PN_UWISH2_012.11515+0.07516 | 272.95467 | -18.40229 | 12.3 | 179.10 | 899.29 | 872.22 | GPSR5 12.116+0.076 |
| PN_UWISH2_012.20907+0.43081 | 272.67407 | -18.14868 | 5.2 | 36.29 | 93.15 | 87.46 | New |
| PN_UWISH2_012.21971-0.33477 | 273.38671 | -18.50730 | 10.8 | 67.23 | 241.45 | 198.28 | New |
| PN_UWISH2_012.71728+0.37202 | 272.98548 | -17.73160 | 7.6 | 105.71 | 403.04 | 372.10 | New |
| PN_UWISH2_012.80348+0.00510 | 273.36698 | -17.83207 | 16.9 | 144.48 | 463.28 | 427.44 | New |
| PN_UWISH2_013.61090+1.01274 | 272.84745 | -16.64001 | 9.2 | 145.48 | 820.75 | 699.76 | New |
| PN_UWISH2_014.58523+0.46161 | 273.83795 | -16.04881 | 7.4 | 56.81 | 247.96 | 213.56 | PN G014.5+00.4 |
| PN_UWISH2_014.64501+0.08920 | 274.20847 | -16.17352 | 10.4 | 85.77 | 317.09 | 321.64 | New |
| PN_UWISH2_014.65833+1.01220 | 273.37138 | -15.72154 | 18.8 | 186.94 | 887.33 | 882.35 | PN G014.6+01.0 |
| PN_UWISH2_014.92112+0.06989 | 274.36260 | -15.93970 | 17.5 | 101.11 | 384.56 | 385.95 | IRAS 18145-1557 |
| PN_UWISH2_015.13012-0.44046 | 274.93310 | -15.99718 | 30.5 | 368.79 | 1810.59 | 1662.43 | New |
| PN_UWISH2_015.53753-0.01923 | 274.74746 | -15.43907 | 29.9 | 43.62 | 189.24 | 178.44 | PN G015.5-00.0 |
| PN_UWISH2_015.54859-1.00657 | 275.65740 | -15.89444 | 8.5 | 73.78 | 414.18 | 379.23 | IRAS 18197-1555 |
| PN_UWISH2_015.67993-1.36320 | 276.04901 | -15.94546 | 11.4 | 150.86 | 693.24 | 629.09 | New |
| PN_UWISH2_016.02790-1.00525 | 275.88952 | -15.47051 | 4.7 | 41.72 | 152.10 | 146.44 | New |
| PN_UWISH2_016.11984-0.98789 | 275.91826 | -15.38115 | 16.6 | 110.13 | 255.34 | 259.28 | New |
| PN_UWISH2_016.17480+1.37914 | 273.78738 | -14.21429 | 12.5 | 114.53 | 345.46 | 350.14 | New |
| PN_UWISH2_016.41571-0.93047 | 276.00920 | -15.09285 | 32.3 | 326.45 | 1539.81 | 1349.89 | PN G016.4-00.9 |
| PN_UWISH2_016.48834-1.36082 | 276.43858 | -15.22966 | 33.8 | 188.83 | 570.06 | 557.68 | New |
| PN_UWISH2_016.60078-0.27565 | 275.50065 | -14.62230 | 8.5 | 101.08 | 461.29 | 411.40 | New |
| PN_UWISH2_016.92321-0.00616 | 275.41159 | -14.21103 | 6.7 | 64.19 | 185.62 | 179.73 | New |

Continued on next page

Table B1 – continued from previous page

| Source ID | RA [deg] | DEC [deg] | Radius [arcsec] | Area [arcsec ²] | F_{tot} [10^{-19}Wm^{-2}] | F_{med} | Other ID |
|-----------------------------|-------------|--------------|--------------------|--------------------------------|--|-----------|---------------------------|
| PN_UWISH2_017.22288+0.12645 | 275.43624 | -13.88420 | 37.3 | 232.61 | 1324.38 | 790.29 | PN G017.2+00.1 |
| PN_UWISH2_017.58861+1.09048 | 274.73927 | -13.10716 | 7.8 | 72.61 | 282.56 | 256.31 | New |
| PN_UWISH2_017.61528-1.17013 | 276.80657 | -14.14383 | 152.8 | 6864.53 | 330258.97 | 85111.55 | PN G017.6-01.1 |
| PN_UWISH2_018.14941+1.53214 | 274.61205 | -12.40431 | 9.9 | 73.37 | 356.23 | 285.41 | PN G018.1+01.5 |
| PN_UWISH2_018.41760-0.10793 | 276.22489 | -12.93880 | 14.8 | 250.57 | 7524.71 | 1420.73 | New |
| PN_UWISH2_018.83207+0.48278 | 275.88871 | -12.29607 | 3.6 | 29.65 | 193.62 | 182.94 | New |
| PN_UWISH2_020.46958+0.67836 | 276.49348 | -10.75715 | 31.0 | 144.90 | 497.17 | 474.42 | PN G020.4+00.6 |
| PN_UWISH2_020.70907-0.17267 | 277.37398 | -10.94099 | 12.9 | 261.67 | 1516.99 | 1431.33 | New |
| PN_UWISH2_020.80590-0.57267 | 277.78078 | -11.04048 | 16.4 | 202.93 | 898.55 | 855.13 | New |
| PN_UWISH2_020.85450+0.48588 | 276.84922 | -10.50625 | 2.4 | 10.67 | 108.07 | 67.97 | SSTGLMC G020.8543+00.4857 |
| PN_UWISH2_020.97795+0.92363 | 276.51391 | -10.19310 | 28.1 | 137.21 | 684.15 | 592.45 | GPSR 020.979+0.925 |
| PN_UWISH2_020.98141+0.85244 | 276.57954 | -10.22323 | 25.7 | 293.44 | 1726.19 | 1527.14 | MHO 3200 |
| PN_UWISH2_021.29383+0.98091 | 276.61194 | -9.88697 | 9.6 | 109.65 | 417.59 | 382.68 | PN G021.2+00.9 |
| PN_UWISH2_021.30767-0.25089 | 277.72679 | -10.44677 | 22.0 | 103.42 | 303.70 | 295.95 | New |
| PN_UWISH2_021.74338-0.67287 | 278.31186 | -10.25536 | 14.0 | 211.85 | 1983.87 | 1480.83 | PN G021.7-00.6 |
| PN_UWISH2_021.81951-0.47837 | 278.17225 | -10.09807 | 26.3 | 429.56 | 2257.37 | 2074.66 | PN G021.8-00.4 |
| PN_UWISH2_022.44734-0.44228 | 278.43371 | -9.52442 | 25.3 | 165.39 | 608.36 | 580.98 | New |
| PN_UWISH2_022.57000+1.05505 | 277.14674 | -8.72291 | 13.1 | 289.63 | 3901.84 | 3278.61 | PN G022.5+01.0 |
| PN_UWISH2_022.99501-0.56968 | 278.80394 | -9.09703 | 7.8 | 83.05 | 255.30 | 243.34 | New |
| PN_UWISH2_022.99982+0.10714 | 278.19818 | -8.78078 | 22.7 | 183.99 | 666.78 | 624.85 | New |
| PN_UWISH2_023.44011+0.74528 | 277.83172 | -8.09545 | 10.4 | 160.99 | 996.94 | 898.32 | PN G023.4+00.7 |
| PN_UWISH2_023.78286+0.50238 | 278.20917 | -7.90372 | 3.5 | 23.67 | 126.19 | 106.99 | New |
| PN_UWISH2_023.89021-0.73778 | 279.37125 | -8.37930 | 12.8 | 158.79 | 426.44 | 567.42 | GPSR 023.890-0.737 |
| PN_UWISH2_023.90016-1.28024 | 279.86330 | -8.61917 | 13.6 | 238.74 | 1905.40 | 1258.16 | PN G023.9-01.2 |
| PN_UWISH2_024.58540+0.11989 | 278.92479 | -7.36772 | 7.8 | 43.53 | 162.26 | 138.43 | New |
| PN_UWISH2_024.76272-0.91396 | 279.93336 | -7.68478 | 2.8 | 16.29 | 110.21 | 97.41 | New |
| PN_UWISH2_024.77483-1.31616 | 280.29988 | -7.85808 | 41.4 | 93.54 | 261.05 | 256.44 | MHO 2456 |
| PN_UWISH2_024.89596+0.45853 | 278.76581 | -6.93617 | 9.2 | 118.28 | 341.25 | 891.83 | G024.8959+00.4586 |
| PN_UWISH2_025.66408+1.15020 | 278.50388 | -5.93589 | 28.4 | 151.60 | 402.43 | 414.26 | PN G025.6+01.1 |
| PN_UWISH2_025.77993-0.44005 | 279.97837 | -6.56355 | 4.1 | 37.20 | 284.64 | 231.01 | New |
| PN_UWISH2_025.92671-0.98449 | 280.53333 | -6.68220 | 10.0 | 106.93 | 1165.94 | 857.58 | PN G025.9-00.9 |
| PN_UWISH2_025.99096-0.59183 | 280.21143 | -6.44546 | 5.5 | 116.81 | 730.31 | 685.15 | New |
| PN_UWISH2_026.42837+1.03759 | 278.95767 | -5.30927 | 5.2 | 35.20 | 144.32 | 124.96 | New |
| PN_UWISH2_026.44767-0.80840 | 280.61536 | -6.13843 | 7.6 | 74.54 | 374.88 | 348.10 | New |
| PN_UWISH2_026.74999-1.21865 | 281.12124 | -6.05692 | 12.8 | 308.77 | 1998.37 | 1713.67 | PN G026.7-01.2 |
| PN_UWISH2_026.79572-1.05024 | 280.99156 | -5.93937 | 13.2 | 201.09 | 1233.94 | 1023.55 | PN G026.8-01.0 |
| PN_UWISH2_026.83269-0.15180 | 280.20553 | -5.49569 | 6.9 | 66.40 | 490.11 | 436.91 | PN G026.8-00.1 |
| PN_UWISH2_026.83640+0.28828 | 279.81431 | -5.29077 | 4.9 | 42.57 | 316.53 | 310.34 | New |
| PN_UWISH2_027.09954+0.94886 | 279.34624 | -4.75395 | 6.8 | 75.15 | 233.94 | 226.95 | New |
| PN_UWISH2_027.37280+1.39262 | 279.07660 | -4.30750 | 4.1 | 21.17 | 60.48 | 62.66 | New |
| PN_UWISH2_027.66357-0.82670 | 281.18977 | -5.06529 | 11.7 | 137.45 | 664.66 | 598.03 | PN G027.6-00.8 |
| PN_UWISH2_027.70327+0.70354 | 279.84264 | -4.33003 | 37.4 | 386.40 | 1632.32 | 1556.50 | PN G027.7+00.7 |
| PN_UWISH2_027.81843-0.76628 | 281.20679 | -4.89994 | 7.1 | 56.83 | 318.47 | 289.26 | PN G027.8-00.7 |
| PN_UWISH2_028.06295-0.61048 | 281.17972 | -4.61128 | 4.9 | 34.62 | 137.77 | 132.94 | New |
| PN_UWISH2_028.19767-0.89109 | 281.49190 | -4.61951 | 11.7 | 61.46 | 164.11 | 161.12 | New |
| PN_UWISH2_028.52225-1.48422 | 282.16994 | -4.60108 | 30.4 | 99.29 | 274.33 | 277.01 | PN G028.5-01.4 |
| PN_UWISH2_028.62122-0.86537 | 281.66273 | -4.23091 | 7.7 | 29.57 | 63.90 | 65.83 | New |
| PN_UWISH2_028.89451-0.29151 | 281.27590 | -3.72585 | 32.6 | 202.61 | 780.88 | 762.12 | PN G028.8-00.2 |
| PN_UWISH2_029.21554+0.02262 | 281.14282 | -3.29679 | 22.0 | 215.51 | 2369.65 | 711.76 | New |
| PN_UWISH2_029.50204+0.62395 | 280.73827 | -2.76719 | 15.6 | 316.05 | 1600.87 | 1607.46 | PN G029.5+00.6 |
| PN_UWISH2_029.57883-0.26901 | 281.56882 | -3.10673 | 6.1 | 49.36 | 258.66 | 660.93 | PN G029.5-00.2 |
| PN_UWISH2_029.99765+0.65621 | 280.93623 | -2.31163 | 5.6 | 55.76 | 351.46 | 325.64 | G30.421-0.226 |
| PN_UWISH2_030.04497+0.03465 | 281.51132 | -2.55337 | 31.1 | 452.87 | 1929.37 | 1880.83 | PN G030.0+00.0 |
| PN_UWISH2_030.17049+0.68782 | 280.98710 | -2.14346 | 5.9 | 54.68 | 356.97 | 300.21 | New |
| PN_UWISH2_030.22594+0.54285 | 281.14150 | -2.16034 | 14.0 | 108.68 | 414.40 | 398.18 | New |
| PN_UWISH2_030.30097-1.22812 | 282.75329 | -2.90143 | 9.0 | 78.48 | 351.91 | 292.73 | New |
| PN_UWISH2_030.50743-0.21913 | 281.94856 | -2.25769 | 17.0 | 199.62 | 943.44 | 847.33 | PN G030.5-00.2 |
| PN_UWISH2_030.66759-0.33136 | 282.12162 | -2.16634 | 11.7 | 76.83 | 399.40 | 322.69 | G030.6671-00.3316 |
| PN_UWISH2_030.72160+0.14788 | 281.71954 | -1.89964 | 14.9 | 100.07 | 270.46 | 280.51 | New |
| PN_UWISH2_030.76828+1.40983 | 280.61768 | -1.28196 | 3.7 | 24.77 | 126.92 | 114.19 | New |
| PN_UWISH2_031.16908+0.81029 | 281.33422 | -1.19919 | 3.3 | 22.97 | 95.06 | 90.50 | New |
| PN_UWISH2_031.32618-0.53286 | 282.60153 | -1.67212 | 44.9 | 592.19 | 3797.09 | 3019.22 | PN G031.3-00.5 |
| PN_UWISH2_031.63781+0.99595 | 281.38290 | -0.69744 | 6.6 | 62.40 | 389.78 | 344.45 | New |
| PN_UWISH2_031.90685-0.30936 | 282.66738 | -1.05343 | 27.7 | 368.30 | 2400.90 | 2183.65 | PN G031.9-00.3 |

Continued on next page

Table B1 – continued from previous page

| Source ID | RA [deg] | DEC [deg] | Radius [arcsec] | Area [arcsec ²] | F_{tot} [$10^{-19}Wm^{-2}$] | F_{med} | Other ID |
|-----------------------------|-------------|--------------|--------------------|--------------------------------|------------------------------------|-----------|-------------------------|
| PN_UWISH2_032.14993+0.64445 | 281.92933 | -0.40212 | 7.6 | 62.99 | 300.67 | 251.96 | New |
| PN_UWISH2_032.22860-1.44045 | 283.82102 | -1.28266 | 30.1 | 211.09 | 597.61 | 614.37 | PN G032.2-01.4 |
| PN_UWISH2_032.28479-0.27816 | 282.81195 | -0.70284 | 7.2 | 91.60 | 477.47 | 438.76 | New |
| PN_UWISH2_032.29224-0.74568 | 283.23149 | -0.90936 | 4.1 | 29.38 | 231.96 | 173.05 | New |
| PN_UWISH2_032.37721-0.55490 | 283.10042 | -0.74677 | 7.6 | 79.64 | 444.97 | 406.96 | PN G032.3-00.5 |
| PN_UWISH2_032.46866+0.28147 | 282.39772 | -0.28401 | 6.6 | 53.49 | 199.32 | 171.17 | New |
| PN_UWISH2_032.54650-0.03210 | 282.71230 | -0.35773 | 17.9 | 281.26 | 2062.73 | 1760.69 | PN G032.5-00.0 |
| PN_UWISH2_032.54998-0.29529 | 282.94812 | -0.47464 | 12.5 | 219.21 | 1571.41 | 1552.01 | PN G032.5-00.3 |
| PN_UWISH2_032.61348+0.79678 | 282.00515 | +0.07986 | 3.8 | 31.65 | 241.38 | 160.47 | PN PM 1-258 |
| PN_UWISH2_032.66916-1.25559 | 283.85720 | -0.80638 | 10.2 | 124.80 | 973.71 | 817.44 | PN G032.6-01.2 |
| PN_UWISH2_032.94004-0.74662 | 283.52766 | -0.33328 | 7.9 | 102.73 | 759.84 | 697.54 | PN G032.9-00.7 |
| PN_UWISH2_033.16509+0.49150 | 282.52836 | +0.43156 | 3.8 | 25.56 | 106.84 | 108.63 | New |
| PN_UWISH2_033.45470-0.61500 | 283.64519 | +0.18474 | 4.8 | 24.37 | 27.24 | 76.77 | PN G033.4-00.6 |
| PN_UWISH2_033.88796+1.52134 | 281.94106 | +1.54427 | 33.8 | 86.69 | 255.42 | 247.80 | PN G033.8+01.5 |
| PN_UWISH2_033.97946-0.98557 | 284.21432 | +0.48266 | 2.2 | 4.42 | 8.03 | 8.88 | PN G033.9-00.9 |
| PN_UWISH2_034.10462-1.64333 | 284.85672 | +0.29388 | 12.0 | 148.05 | 1176.28 | 1034.87 | PN G034.1-01.6 |
| PN_UWISH2_034.41021+0.81477 | 282.80828 | +1.68706 | 4.5 | 36.56 | 115.32 | 110.41 | New |
| PN_UWISH2_034.84509+1.31721 | 282.55901 | +2.30305 | 9.1 | 125.35 | 698.43 | 611.71 | New |
| PN_UWISH2_035.18522+1.12134 | 282.88860 | +2.51653 | 11.5 | 43.14 | 107.63 | 103.53 | New |
| PN_UWISH2_035.23366-1.13623 | 284.92089 | +1.52961 | 30.0 | 120.64 | 251.39 | 255.44 | New |
| PN_UWISH2_035.38919-1.17506 | 285.02650 | +1.65019 | 12.0 | 122.81 | 375.93 | 372.11 | New |
| PN_UWISH2_035.47394-0.43716 | 284.40844 | +2.06260 | 20.9 | 292.90 | 1251.38 | 1039.51 | IRAS 18551+0159 |
| PN_UWISH2_035.76967-1.24531 | 285.26293 | +1.95644 | 16.6 | 461.29 | 3353.90 | 2827.71 | New |
| PN_UWISH2_035.81426+1.48019 | 282.85558 | +3.23983 | 11.8 | 75.27 | 181.05 | 183.03 | New |
| PN_UWISH2_035.81489-0.25181 | 284.39919 | +2.45055 | 15.6 | 279.99 | 850.69 | 834.37 | New |
| PN_UWISH2_035.89918-1.14425 | 285.23222 | +2.11780 | 4.9 | 44.77 | 196.69 | 182.66 | New |
| PN_UWISH2_036.05309-1.36593 | 285.49991 | +2.15329 | 149.5 | 4344.13 | 22362.90 | 20233.61 | PN G035.9-01.1 |
| PN_UWISH2_036.43225-1.91396 | 286.16112 | +2.23949 | 1.7 | 4.02 | 58.24 | 30.95 | PN G036.4-01.9 |
| PN_UWISH2_036.46081+0.80581 | 283.75199 | +3.50792 | 10.5 | 47.01 | 71.59 | 73.22 | New |
| PN_UWISH2_036.48189+0.15610 | 284.34075 | +3.23021 | 8.9 | 98.54 | 440.57 | 369.52 | New |
| PN_UWISH2_036.98479-0.20330 | 284.89114 | +3.51340 | 7.2 | 106.23 | 311.99 | 290.01 | New |
| PN_UWISH2_037.14125+0.30341 | 284.51110 | +3.88408 | 6.8 | 55.62 | 138.70 | 135.16 | New |
| PN_UWISH2_037.41544-0.19254 | 285.07885 | +3.90133 | 5.0 | 55.13 | 365.57 | 311.48 | New |
| PN_UWISH2_037.96134+0.45337 | 284.75297 | +4.68210 | 7.2 | 50.18 | 257.08 | 243.87 | MSX6C G037.9595+00.4535 |
| PN_UWISH2_038.14463-0.57489 | 285.75429 | +4.37465 | 6.5 | 66.25 | 255.38 | 257.05 | New |
| PN_UWISH2_038.83959+0.87057 | 284.78315 | +5.65389 | 5.5 | 51.95 | 200.06 | 197.93 | New |
| PN_UWISH2_039.16222+0.78375 | 285.00892 | +5.90117 | 7.1 | 24.74 | 54.26 | 45.90 | New |
| PN_UWISH2_039.26101-0.55123 | 286.24689 | +5.37758 | 13.8 | 100.73 | 252.46 | 253.89 | New |
| PN_UWISH2_039.64158-0.36822 | 286.25902 | +5.79968 | 4.3 | 37.29 | 208.89 | 170.42 | New |
| PN_UWISH2_040.03148-1.30313 | 287.27361 | +5.71599 | 29.0 | 42.09 | 86.46 | 82.29 | GPSR 040.033-1.302 |
| PN_UWISH2_040.36950-0.47517 | 286.69085 | +6.39710 | 32.2 | 1195.79 | 2682.48 | 9475.86 | PN G040.3-00.4 |
| PN_UWISH2_040.47073+1.10067 | 285.32726 | +7.20967 | 7.6 | 76.14 | 797.05 | 546.69 | New |
| PN_UWISH2_040.53948-0.76310 | 287.02679 | +6.41554 | 8.0 | 144.08 | 050.63 | 1022.97 | New |
| PN_UWISH2_040.96700-1.22601 | 287.63857 | +6.58146 | 61.5 | 382.13 | 1021.97 | 1026.43 | New |
| PN_UWISH2_041.27043-0.69797 | 287.30768 | +7.09423 | 16.3 | 405.50 | 3270.84 | 2883.10 | PN G041.2-00.6 |
| PN_UWISH2_041.99634+0.10743 | 286.92389 | +8.10956 | 19.9 | 16.17 | 24.70 | 26.29 | New |
| PN_UWISH2_042.12631+0.45706 | 286.67062 | +8.38580 | 9.0 | 126.16 | 547.41 | 509.69 | New |
| PN_UWISH2_042.97101-1.07103 | 288.43505 | +8.42942 | 4.9 | 38.11 | 152.55 | 146.72 | New |
| PN_UWISH2_043.10420-1.70207 | 289.06236 | +8.25419 | 9.8 | 68.68 | 172.42 | 174.90 | New |
| PN_UWISH2_043.25830+1.50423 | 286.25472 | +9.87206 | 5.5 | 40.78 | 191.80 | 134.57 | New |
| PN_UWISH2_043.65562-0.82777 | 288.53841 | +9.14866 | 4.0 | 39.85 | 194.97 | 196.86 | New |
| PN_UWISH2_044.18877+1.56732 | 286.63144 | +10.72749 | 100.4 | 1127.24 | 16445.03 | 2750.69 | PN G044.1+01.5 |
| PN_UWISH2_044.34714+0.08637 | 288.04202 | +10.18518 | 6.1 | 73.84 | 187.67 | 177.95 | New |
| PN_UWISH2_044.73433+0.26046 | 288.06742 | +10.60898 | 16.1 | 325.33 | 3884.71 | 3071.11 | PN G044.7+00.2 |
| PN_UWISH2_044.93245-0.01060 | 288.40523 | +10.65887 | 27.7 | 859.52 | 5722.84 | 4532.10 | PN G044.9+00.0 |
| PN_UWISH2_045.44425-1.57085 | 290.05177 | +10.38386 | 11.0 | 50.65 | 83.50 | 84.33 | New |
| PN_UWISH2_045.45878-0.49801 | 289.09365 | +10.89817 | 31.3 | 186.85 | 443.03 | 433.85 | New |
| PN_UWISH2_045.95707+0.69049 | 288.25641 | +11.89176 | 21.8 | 192.00 | 504.54 | 445.28 | New |
| PN_UWISH2_046.09523+1.36603 | 287.70922 | +12.32673 | 5.8 | 53.80 | 157.90 | 140.96 | New |
| PN_UWISH2_046.63335+1.31220 | 288.01280 | +12.77895 | 6.8 | 90.48 | 323.00 | 294.06 | New |
| PN_UWISH2_046.93735-0.54973 | 289.84548 | +12.18115 | 5.4 | 43.42 | 204.57 | 180.63 | New |
| PN_UWISH2_047.18522+0.44999 | 289.05872 | +12.86745 | 14.3 | 367.10 | 1724.42 | 1558.36 | New |
| PN_UWISH2_047.44521+0.61199 | 289.03591 | +13.17296 | 5.8 | 70.25 | 212.27 | 191.78 | New |
| PN_UWISH2_047.50612-0.36750 | 289.95370 | +12.76896 | 15.1 | 188.00 | 982.46 | 827.20 | New |

Continued on next page

Table B1 – continued from previous page

| Source ID | RA [deg] | DEC [deg] | Radius [arcsec] | Area [arcsec ²] | F_{tot} [10^{-19}Wm^{-2}] | F_{med} | Other ID |
|-----------------------------|-------------|--------------|--------------------|--------------------------------|--|-----------|----------------------------|
| PN_UWISH2_047.52536+0.32144 | 289.33823 | +13.10836 | 7.5 | 68.59 | 245.39 | 244.87 | New |
| PN_UWISH2_047.61228+1.08168 | 288.68845 | +13.53933 | 11.4 | 212.69 | 926.61 | 903.93 | PN G047.6+01.0 |
| PN_UWISH2_048.03497+0.12296 | 289.76335 | +13.46599 | 7.1 | 73.77 | 205.19 | 185.16 | New |
| PN_UWISH2_048.24968-0.46947 | 290.40474 | +13.37742 | 12.3 | 152.83 | 747.66 | 539.49 | New |
| PN_UWISH2_048.71570-0.28960 | 290.46721 | +13.87323 | 25.4 | 364.39 | 2620.46 | 2407.63 | PN G048.7-00.2 |
| PN_UWISH2_048.99884+0.77703 | 289.63259 | +14.62389 | 16.9 | 240.14 | 1116.38 | 1035.00 | New |
| PN_UWISH2_049.28561+0.00740 | 290.47382 | +14.51586 | 46.3 | 569.06 | 2981.11 | 2487.01 | PN G049.2+00.0 |
| PN_UWISH2_049.86763+1.06075 | 289.79393 | +15.52434 | 18.8 | 88.86 | 197.54 | 208.44 | New |
| PN_UWISH2_049.91632-1.08675 | 291.77791 | +14.55322 | 7.5 | 93.90 | 684.22 | 413.16 | New |
| PN_UWISH2_050.04556-0.79804 | 291.57794 | +14.80423 | 11.8 | 168.42 | 916.59 | 828.63 | New |
| PN_UWISH2_050.48027+0.70434 | 290.41955 | +15.89793 | 10.0 | 53.94 | 406.30 | 265.92 | PN G050.4+00.7 |
| PN_UWISH2_050.55559+0.04506 | 291.06046 | +15.65315 | 13.4 | 151.83 | 1031.51 | 822.92 | MSX6C G050.5557+00.0448 |
| PN_UWISH2_050.66579+1.33631 | 289.92941 | +16.35846 | 4.6 | 25.36 | 158.23 | 146.07 | NVSS J191942+162128 |
| PN_UWISH2_050.66912+0.00673 | 291.15137 | +15.73500 | 14.9 | 296.54 | 1740.80 | 1598.35 | PN G050.6+0.00 |
| PN_UWISH2_050.71285-0.17840 | 291.34224 | +15.68573 | 4.1 | 22.96 | 57.61 | 54.64 | SSTGLMC G050.7128-00.1780 |
| PN_UWISH2_050.78036+1.18512 | 290.12457 | +16.38873 | 13.0 | 76.08 | 163.43 | 159.22 | New |
| PN_UWISH2_050.90936+1.05076 | 290.31138 | +16.43949 | 4.2 | 28.91 | 113.63 | 79.79 | New |
| PN_UWISH2_050.92866+0.43874 | 290.88325 | +16.16805 | 8.8 | 97.01 | 326.21 | 328.86 | New |
| PN_UWISH2_051.36290+0.87878 | 290.69251 | +16.75857 | 4.8 | 53.32 | 350.03 | 319.39 | New |
| PN_UWISH2_051.50791+0.17037 | 291.41553 | +16.55106 | 11.4 | 126.26 | 578.84 | 398.98 | PN G051.5+00.2 |
| PN_UWISH2_051.76939+1.36491 | 290.44421 | +17.34605 | 7.9 | 47.35 | 88.78 | 91.94 | PN G051.7+01.3 |
| PN_UWISH2_051.83306+0.28374 | 291.47259 | +16.89104 | 2.6 | 8.95 | 116.17 | 80.64 | PN G051.8+00.2 |
| PN_UWISH2_052.32654-0.13737 | 292.10564 | +17.12427 | 7.3 | 71.74 | 208.44 | 211.63 | New |
| PN_UWISH2_052.46943-0.90047 | 292.87751 | +16.88365 | 6.1 | 50.84 | 188.75 | 175.91 | New |
| PN_UWISH2_052.70187-1.04355 | 293.12567 | +17.01832 | 15.2 | 39.27 | 57.60 | 55.43 | New |
| PN_UWISH2_053.04316-0.06957 | 292.40274 | +17.78595 | 8.7 | 96.71 | 561.10 | 420.69 | New |
| PN_UWISH2_053.36023-0.54988 | 293.00521 | +17.83310 | 7.5 | 57.09 | 185.39 | 169.56 | New |
| PN_UWISH2_054.29190-0.23778 | 293.19088 | +18.79969 | 13.7 | 140.74 | 452.81 | 408.15 | New |
| PN_UWISH2_054.71154+0.41990 | 292.79511 | +19.48442 | 13.3 | 188.23 | 750.03 | 725.44 | PN G054.7+00.4 |
| PN_UWISH2_055.50747-0.55729 | 294.11183 | +19.70728 | 11.7 | 63.20 | 136.06 | 139.41 | PN G055.5-00.5 |
| PN_UWISH2_055.85017+1.44210 | 292.42181 | +20.97381 | 3.5 | 14.40 | 91.78 | 33.55 | IRAS 19275+2052 |
| PN_UWISH2_056.16673-0.41918 | 294.32630 | +20.34998 | 25.6 | 152.88 | 544.46 | 501.19 | PN G056.1-00.4 |
| PN_UWISH2_056.34479-1.53764 | 295.45680 | +19.95462 | 22.9 | 244.36 | 688.72 | 737.19 | New |
| PN_UWISH2_056.42331-0.37341 | 294.41770 | +20.59614 | 15.7 | 36.70 | 140.07 | 135.03 | PN G056.4-00.3 |
| PN_UWISH2_056.48535-0.09364 | 294.18926 | +20.78706 | 7.4 | 56.97 | 490.79 | 251.81 | New |
| PN_UWISH2_056.52321+0.30702 | 293.83452 | +21.01540 | 7.6 | 25.68 | 60.67 | 59.06 | New |
| PN_UWISH2_056.61303-0.04761 | 294.21301 | +20.92095 | 10.8 | 75.07 | 143.00 | 144.35 | New |
| PN_UWISH2_057.32913+0.61698 | 293.96505 | +21.87025 | 3.5 | 12.70 | 35.54 | 35.18 | New |
| PN_UWISH2_057.59474+0.50715 | 294.20811 | +22.04854 | 71.8 | 168.49 | 474.72 | 380.17 | New |
| PN_UWISH2_057.64365+0.47814 | 294.26120 | +22.07705 | 15.7 | 49.74 | 106.16 | 108.30 | New |
| PN_UWISH2_057.72078+0.12541 | 294.63369 | +21.97154 | 3.2 | 10.74 | 21.34 | 23.41 | New |
| PN_UWISH2_057.81415+0.78641 | 294.06045 | +22.37632 | 11.2 | 16.38 | 34.10 | 33.73 | New |
| PN_UWISH2_057.83552+1.04920 | 293.82333 | +22.52291 | 15.7 | 161.92 | 612.56 | 595.87 | PN G057.8+01.0 |
| PN_UWISH2_057.98004-0.76740 | 295.60822 | +21.75634 | 16.7 | 434.52 | 4950.65 | 3888.95 | PN G057.9-00.7 |
| PN_UWISH2_058.03770-0.04866 | 294.96541 | +22.16189 | 12.4 | 118.13 | 711.13 | 409.12 | New |
| PN_UWISH2_058.17873-0.81177 | 295.75604 | +21.90672 | 17.2 | 160.93 | 769.03 | 707.50 | IPHASX J194301.3+215424 |
| PN_UWISH2_058.80916+0.38692 | 294.96654 | +23.04782 | 19.2 | 225.19 | 613.84 | 632.41 | New |
| PN_UWISH2_059.18828-1.42144 | 296.87169 | +22.47539 | 16.1 | 183.33 | 669.01 | 647.15 | PN G059.1-01.4 |
| PN_UWISH2_059.36328+1.00137 | 294.68039 | +23.83244 | 3.0 | 7.63 | 22.54 | 23.88 | New |
| PN_UWISH2_059.77812-0.82788 | 296.63714 | +23.28371 | 9.7 | 177.59 | 4307.78 | 1662.24 | PN G059.7-00.8 |
| PN_UWISH2_059.87554-0.60874 | 296.48399 | +23.47800 | 25.3 | 172.51 | 557.42 | 557.70 | PN G059.8-00.6 |
| PN_UWISH2_060.24810+0.82261 | 295.32874 | +24.51420 | 32.1 | 185.63 | 879.93 | 762.55 | Kronberger GN J1941.3+2430 |
| PN_UWISH2_060.31487+0.79769 | 295.38886 | +24.55989 | 2.6 | 11.74 | 49.98 | 47.90 | New |
| PN_UWISH2_060.40130+0.97372 | 295.26758 | +24.72207 | 9.5 | 91.77 | 219.05 | 219.33 | New |
| PN_UWISH2_060.52372-0.31828 | 296.56513 | +24.18437 | 7.3 | 103.74 | 1170.77 | 1066.45 | PN G060.5-00.3 |
| PN_UWISH2_060.79926+1.17327 | 295.29316 | +25.16660 | 4.2 | 13.28 | 25.83 | 26.96 | New |
| PN_UWISH2_061.84215+0.88506 | 296.14467 | +25.92826 | 10.2 | 191.11 | 887.07 | 705.20 | New |
| PN_UWISH2_061.91270+0.20109 | 296.84101 | +25.64602 | 7.5 | 108.16 | 330.31 | 305.01 | New |
| PN_UWISH2_062.07780-0.43633 | 297.54294 | +25.46559 | 17.1 | 81.06 | 149.06 | 150.19 | New |
| PN_UWISH2_062.13719+0.14857 | 297.01712 | +25.81331 | 7.0 | 119.67 | 606.13 | 503.81 | New |
| PN_UWISH2_062.15368+1.15140 | 296.06083 | +26.33111 | 7.1 | 66.06 | 136.15 | 138.73 | New |
| PN_UWISH2_062.29042+1.13629 | 296.15164 | +26.44203 | 9.4 | 156.43 | 989.99 | 905.73 | New |
| PN_UWISH2_062.45283-0.01779 | 297.35430 | +26.00125 | 13.0 | 171.08 | 555.39 | 535.48 | New |
| PN_UWISH2_062.49346-0.27008 | 297.61889 | +25.90799 | 45.4 | 489.22 | 1341.03 | 1237.50 | PN G062.4-00.2 |

Continued on next page

Table B1 – continued from previous page

| Source ID | RA [deg] | DEC [deg] | Radius [arcsec] | Area [arcsec ²] | F_{tot} [10^{-19}Wm^{-2}] | F_{med} | Other ID |
|-----------------------------|-------------|--------------|--------------------|--------------------------------|--|-----------|---------------------------|
| PN_UWISH2_062.70165+0.06019 | 297.42017 | +26.25520 | 12.6 | 248.72 | 2127.60 | 1395.32 | PN G062.7+00.0 |
| PN_UWISH2_062.75413-0.72565 | 298.20231 | +25.89915 | 41.1 | 309.48 | 1031.28 | 963.32 | PN G062.7-00.7 |
| PN_UWISH2_062.97476+1.38380 | 296.29463 | +27.15831 | 9.1 | 147.33 | 1006.81 | 864.83 | PN G062.9+01.3 |
| PN_UWISH2_063.92454-1.21740 | 299.34644 | +26.64663 | 20.3 | 71.19 | 123.18 | 107.66 | TEUTSCH PN J1957.3+2639 |
| PN_UWISH2_064.13697-0.97667 | 299.24006 | +26.95330 | 15.2 | 279.17 | 938.35 | 874.99 | IPHASX J195657.6+265713 |
| PN_UWISH2_064.18792+0.77438 | 297.57807 | +27.89812 | 6.9 | 93.23 | 886.65 | 602.27 | New |
| PN_UWISH2_064.29941-0.14559 | 298.53508 | +27.52268 | 21.9 | 282.35 | 840.34 | 812.91 | New |
| PN_UWISH2_064.94759+0.76048 | 298.03161 | +28.54425 | 8.1 | 79.97 | 334.74 | 259.10 | New |
| PN_UWISH2_065.54459+0.81855 | 298.32416 | +29.08648 | 9.8 | 110.56 | 333.96 | 331.68 | New |
| PN_UWISH2_075.90338+0.29517 | 305.56985 | +37.51621 | 6.2 | 37.98 | 147.45 | 138.63 | IRAS 20204+3721 |
| PN_UWISH2_076.37264+1.17216 | 304.99291 | +38.40071 | 28.0 | 937.52 | 4816.41 | 4462.80 | PN G076.3+01.1 |
| PN_UWISH2_076.88532+2.22199 | 304.24755 | +39.41480 | 5.5 | 49.81 | 276.23 | 248.05 | New |
| PN_UWISH2_077.65952-0.98321 | 308.18149 | +38.19935 | 10.9 | 17.40 | 20.89 | 20.49 | New |
| PN_UWISH2_077.68068+3.12797 | 303.84237 | +40.57914 | 18.1 | 89.89 | 489.55 | 414.05 | PN G077.7+03.1 |
| PN_UWISH2_077.77375+1.55436 | 305.61335 | +39.77046 | 4.6 | 39.10 | 184.09 | 152.10 | New |
| PN_UWISH2_077.84010+0.86042 | 306.39998 | +39.42610 | 17.1 | 177.79 | 449.55 | 427.28 | New |
| PN_UWISH2_078.92993+0.76378 | 307.32851 | +40.25589 | 9.1 | 195.70 | 3896.91 | 3160.55 | PN G078.9+00.7 |
| PN_UWISH2_079.33319+2.14863 | 306.14806 | +41.38834 | 6.9 | 57.66 | 158.81 | 161.45 | New |
| PN_UWISH2_079.62439+0.40225 | 308.25045 | +40.60291 | 15.5 | 78.42 | 172.78 | 179.45 | New |
| PN_UWISH2_079.77014+1.89347 | 306.76299 | +41.59724 | 4.6 | 42.87 | 82.23 | 83.60 | New |
| PN_UWISH2_080.26214+0.24219 | 308.92358 | +41.01858 | 7.3 | 52.52 | 132.40 | 129.20 | New |
| PN_UWISH2_081.70275+2.15524 | 308.01013 | +43.31551 | 6.9 | 28.75 | 56.09 | 54.25 | New |
| PN_UWISH2_082.02890-0.30589 | 310.94401 | +42.08439 | 6.4 | 70.10 | 134.10 | 134.23 | New |
| PN_UWISH2_084.20031+1.09069 | 311.29225 | +44.65363 | 41.3 | 1754.40 | 13412.66 | 12703.83 | PN G084.2+01.0 |
| PN_UWISH2_084.68426-0.72166 | 313.67853 | +43.87961 | 8.3 | 22.25 | 35.79 | 37.44 | New |
| PN_UWISH2_143.50140-2.81706 | 49.59757 | +54.07942 | 61.1 | 399.82 | 1135.87 | 1091.73 | New |
| PN_UWISH2_144.15931-0.50100 | 52.77255 | +55.64775 | 16.6 | 657.79 | 2599.43 | 2473.29 | BFS 30 |
| PN_UWISH2_146.29327+0.54871 | 56.89683 | +55.22098 | 5.7 | 48.63 | 97.88 | 95.31 | IRAS 03437+5503 |
| PN_UWISH2_149.16730-0.22038 | 59.84500 | +52.80158 | 2.2 | 5.48 | 4.97 | 6.74 | New |
| PN_UWISH2_149.43257-2.19327 | 58.12051 | +51.11816 | 10.5 | 258.08 | 1097.52 | 1094.26 | New |
| PN_UWISH2_151.30910-0.74888 | 61.88161 | +50.98841 | 4.9 | 67.14 | 376.14 | 206.52 | New |
| PN_UWISH2_153.77044-1.40652 | 63.97733 | +48.82783 | 4.7 | 49.03 | 224.19 | 201.51 | PN G153.7-01.4 |
| PN_UWISH2_357.65660+0.26265 | 264.72283 | -30.78903 | 10.0 | 82.48 | 568.19 | 478.38 | New |
| PN_UWISH2_358.23394-1.18468 | 266.51148 | -31.06071 | 19.4 | 489.97 | 6329.42 | 5781.65 | SSTGLMC G358.2595-01.9129 |
| PN_UWISH2_358.25962-1.91267 | 267.25577 | -31.41518 | 7.9 | 73.67 | 1606.15 | 506.11 | New |
| PN_UWISH2_359.35683-0.98000 | 266.98384 | -29.99451 | 28.1 | 567.26 | 21509.73 | 8645.04 | PN G359.3-00.9 |

APPENDIX C: IMAGES TAKEN FOR THE SURVEY

APPENDIX D: COMPLETE H₂ SOURCE LIST

Table D1: Table listing all the extended H_2 features in our survey. We list the following columns: Source ID which includes the Galactic Coordinates; Right Ascension and Declination in (J2000) system; Area of the H_2 feature; Radius of the H_2 feature; Median surface brightness; Maximum surface brightness; one-pixel rms noise of the background; Total flux of the H_2 feature; Relative flux uncertainty due to photometric calibration; Classification (Jet, PN, SNR or unknown, most likely PDR); Tile name object is on; Image name the object is on; Name of group the object is associated with. This Table is only an excerpt of the first few objects. The full table will be made available online.

| Source ID | RA (J2000) [deg] | DEC [deg] | A [arcsec ²] | r [arcsec] | F_{sb}^{med} [10^{-19} Wm ⁻² arcsec ⁻²] | F_{sb}^{max} [10^{-19} Wm ⁻² arcsec ⁻²] | F_{σ} [10^{-19} Wm ⁻²] | F^{tot} [10^{-19} Wm ⁻²] | $\Delta F/F$ [%] | C | Tile name | Image name | Group name |
|--------------------------|---------------------|--------------|-----------------------------|---------------|--|--|---|--|---------------------|---|--------------|-------------------|------------------------------|
| UWISH2_000.00652+0.15598 | 266.25682 | -28.84930 | 121.51 | 18.4 | 4.26 | 103.44 | 6.13 | 520.11 | 7.9 | u | H2_lm2_15_16 | w20130827_00152_x | PDR_UWISH2_359.99949+0.16099 |
| UWISH2_000.01128+0.16305 | 266.25276 | -28.84155 | 105.35 | 12.3 | 4.17 | 236.49 | 6.21 | 447.16 | 7.9 | u | H2_lm2_15_16 | w20130827_00152_x | PDR_UWISH2_359.99949+0.16099 |
| UWISH2_000.01490+0.16272 | 266.25525 | -28.83864 | 22.97 | 5.3 | 2.39 | 18.70 | 6.31 | 55.68 | 7.9 | u | H2_lm2_15_16 | w20130827_00152_x | PDR_UWISH2_359.99949+0.16099 |
| UWISH2_000.01868+0.16127 | 266.25891 | -28.83617 | 107.44 | 10.3 | 5.54 | 5159.72 | 5.95 | 3916.77 | 7.9 | u | H2_lm2_15_16 | w20130827_00152_x | PDR_UWISH2_359.99949+0.16099 |
| UWISH2_000.02914+0.16027 | 266.26611 | -28.82777 | 45.03 | 5.5 | 3.32 | 227.03 | 6.14 | 122.05 | 7.9 | u | H2_lm2_15_16 | w20130827_00152_x | PDR_UWISH2_359.99949+0.16099 |
| UWISH2_000.03140+0.15965 | 266.26807 | -28.82617 | 7.45 | 3.9 | 2.85 | 52.26 | 5.87 | 20.02 | 7.9 | u | H2_lm2_15_16 | w20130827_00152_x | PDR_UWISH2_359.99949+0.16099 |
| UWISH2_000.03229+0.15892 | 266.26931 | -28.82579 | 5.45 | 2.1 | 4.54 | 15.35 | 4.81 | 24.07 | 7.9 | u | H2_lm2_15_16 | w20130827_00152_x | PDR_UWISH2_359.99949+0.16099 |
| UWISH2_000.03537+0.16025 | 266.26985 | -28.82247 | 34.13 | 5.8 | 2.80 | 43.78 | 5.62 | 109.51 | 7.9 | u | H2_lm2_15_16 | w20130827_00152_x | PDR_UWISH2_359.99949+0.16099 |
| UWISH2_000.03733+0.16046 | 266.27080 | -28.82068 | 5.16 | 1.6 | 4.20 | 20.33 | 5.92 | 24.94 | 7.9 | u | H2_lm2_15_16 | w20130827_00152_x | PDR_UWISH2_359.99949+0.16099 |
| UWISH2_000.03836+0.15947 | 266.27239 | -28.82032 | 6.89 | 2.6 | 3.76 | 17.55 | 4.91 | 31.18 | 7.9 | u | H2_lm2_15_16 | w20130827_00152_x | PDR_UWISH2_359.99949+0.16099 |
| UWISH2_000.03981+0.16052 | 266.27222 | -28.81854 | 6.28 | 2.3 | 4.92 | 42.96 | 5.34 | 33.02 | 7.9 | u | H2_lm2_15_16 | w20130827_00152_x | PDR_UWISH2_359.99949+0.16099 |
| UWISH2_000.04282+0.16170 | 266.27288 | -28.81535 | 97.74 | 10.1 | 4.67 | 83.26 | 5.49 | 460.71 | 7.9 | u | H2_lm2_15_16 | w20130827_00152_x | PDR_UWISH2_359.99949+0.16099 |
| UWISH2_000.05025+0.16283 | 266.63798 | -29.00157 | 142.26 | 11.1 | 3.31 | 40.87 | 5.40 | 473.13 | 8.6 | u | H2_lm2_15_17 | w20130827_00214_w | PDR_UWISH2_000.06358-0.22066 |
| UWISH2_000.08806+0.62191 | 267.06548 | -29.18349 | 9.32 | 3.4 | 3.46 | 49.00 | 5.47 | 134.56 | 3.3 | j | H2_lm2_15_11 | w20130728_00284_y | JET_UWISH2_000.09056-0.65984 |
| UWISH2_000.08823+0.66263 | 267.10553 | -29.20435 | 7.88 | 2.9 | 4.01 | 115.59 | 4.03 | 501.52 | 3.3 | j | H2_lm2_15_11 | w20130728_00284_y | JET_UWISH2_000.09056-0.65984 |
| UWISH2_000.09108+0.66396 | 267.10853 | -29.20259 | 80.40 | 9.0 | 3.45 | 16.82 | 3.82 | 37.24 | 3.3 | j | H2_lm2_15_11 | w20130728_00284_y | JET_UWISH2_000.09056-0.65984 |
| UWISH2_000.11504+0.67902 | 266.73592 | -28.97779 | 36.85 | 5.5 | 5.44 | 235.65 | 5.68 | 205.86 | 8.6 | u | H2_lm2_15_17 | w20130827_00214_w | PDR_UWISH2_000.06358-0.22066 |
| UWISH2_000.12738+0.26989 | 267.14561 | -29.17972 | 38.85 | 7.9 | 3.93 | 18.81 | 3.27 | 35.54 | 3.3 | u | H2_lm2_15_11 | w20130728_00284_y | PDR_UWISH2_000.12738-0.67989 |
| UWISH2_000.16461+0.06333 | 266.44110 | -28.76272 | 79.54 | 10.7 | 8.49 | 296.66 | 7.80 | 803.54 | 10.5 | u | H2_lm2_15_16 | w20130827_00188_x | PDR_UWISH2_000.16461+0.06333 |
| UWISH2_000.16477+0.44615 | 266.93862 | -29.02699 | 166.67 | 13.9 | 3.41 | 62.37 | 3.93 | 771.07 | 10.9 | j | H2_lm2_15_17 | w20130827_00238_w | PDR_UWISH2_000.23142-0.46461 |
| UWISH2_000.20896+0.46070 | 266.97899 | -28.99669 | 6.28 | 2.4 | 4.83 | 16.10 | 3.50 | 30.03 | 10.9 | j | H2_lm2_15_17 | w20130827_00238_w | JET_UWISH2_000.23142-0.46461 |
| UWISH2_000.20910+0.45307 | 266.97160 | -28.99263 | 38.79 | 5.8 | 4.01 | 35.30 | 4.30 | 168.47 | 10.9 | j | H2_lm2_15_17 | w20130827_00238_w | JET_UWISH2_000.23142-0.46461 |
| UWISH2_000.22494+0.47121 | 266.99872 | -28.98844 | 6.56 | 2.7 | 3.05 | 11.15 | 3.17 | 21.34 | 10.9 | j | H2_lm2_15_17 | w20130827_00238_w | JET_UWISH2_000.23142-0.46461 |
| UWISH2_000.22655+0.47021 | 266.99869 | -28.98655 | 25.29 | 4.5 | 2.85 | 15.55 | 3.30 | 76.70 | 10.9 | j | H2_lm2_15_17 | w20130827_00238_w | JET_UWISH2_000.23142-0.46461 |
| UWISH2_000.24117+0.47622 | 267.01321 | -28.97713 | 48.86 | 7.7 | 2.32 | 18.53 | 3.01 | 121.54 | 10.9 | j | H2_lm2_15_17 | w20130827_00238_w | JET_UWISH2_000.23142-0.46461 |
| UWISH2_000.25247+0.47064 | 267.01442 | -28.96458 | 169.46 | 10.8 | 2.57 | 155.29 | 3.07 | 530.41 | 10.9 | j | H2_lm2_15_17 | w20130827_00238_w | JET_UWISH2_000.23142-0.46461 |
| UWISH2_000.26373+0.19745 | 266.75411 | -28.81354 | 253.29 | 14.8 | 5.69 | 2210.84 | 7.39 | 2781.84 | 7.8 | u | H2_lm2_15_17 | w20130827_00226_w | PDR_UWISH2_000.31030-0.20300 |
| UWISH2_000.27057+0.45385 | 267.00868 | -28.94041 | 14.72 | 3.5 | 3.65 | 25.52 | 2.93 | 73.37 | 10.9 | j | H2_lm2_15_17 | w20130827_00238_w | JET_UWISH2_000.23142-0.46461 |
| UWISH2_000.28306+0.47765 | 267.03934 | -28.94201 | 148.32 | 12.6 | 3.80 | 183.74 | 3.05 | 746.67 | 10.9 | j | H2_lm2_15_17 | w20130827_00238_w | JET_UWISH2_000.23142-0.46461 |
| UWISH2_000.30634+0.17076 | 266.75326 | -28.76326 | 53.68 | 7.8 | 3.00 | 115.90 | 3.75 | 335.33 | 7.8 | j | H2_lm2_15_17 | w20130827_00226_w | JET_UWISH2_000.31666-0.18594 |
| UWISH2_000.30904+0.21135 | 266.79447 | -28.78200 | 21.05 | 3.5 | 7.24 | 41.57 | 4.98 | 187.12 | 7.8 | u | H2_lm2_15_17 | w20130827_00226_w | PDR_UWISH2_000.31030-0.20300 |
| UWISH2_000.31508+0.20018 | 266.78715 | -28.77105 | 967.36 | 49.7 | 6.91 | 3377.88 | 4.89 | 16183.15 | 7.8 | u | H2_lm2_15_17 | w20130827_00226_w | PDR_UWISH2_000.31030-0.20300 |
| UWISH2_000.31792+0.19281 | 266.78163 | -28.76480 | 18.46 | 3.7 | 4.84 | 30.59 | 3.34 | 233.24 | 7.8 | u | H2_lm2_15_17 | w20130827_00226_w | PDR_UWISH2_000.31030-0.20300 |
| UWISH2_000.32140+0.22713 | 266.81717 | -28.77960 | 90.22 | 10.3 | 3.70 | 355.74 | 4.18 | 315.07 | 7.8 | u | H2_lm2_15_17 | w20130827_00226_w | PDR_UWISH2_000.31030-0.20300 |
| UWISH2_000.32288+0.20320 | 266.79470 | -28.76594 | 22.45 | 5.0 | 3.08 | 23.90 | 3.86 | 99.16 | 7.8 | j | H2_lm2_15_17 | w20130827_00226_w | JET_UWISH2_000.31666-0.18594 |
| UWISH2_000.32301+0.20783 | 266.79929 | -28.76823 | 70.54 | 8.6 | 3.01 | 16.65 | 3.97 | 200.99 | 7.8 | u | H2_lm2_15_17 | w20130827_00226_w | PDR_UWISH2_000.31030-0.20300 |
| UWISH2_000.32489+0.21032 | 266.80283 | -28.76791 | 19.50 | 4.0 | 4.87 | 41.71 | 3.69 | 133.61 | 7.8 | u | H2_lm2_15_17 | w20130827_00226_w | PDR_UWISH2_000.31030-0.20300 |
| UWISH2_000.32524+0.20528 | 266.79812 | -28.76500 | 102.03 | 9.7 | 2.57 | 18.15 | 3.93 | 51.46 | 7.8 | u | H2_lm2_15_17 | w20130827_00226_w | PDR_UWISH2_000.31030-0.20300 |
| UWISH2_000.32696+0.19658 | 266.79066 | -28.75902 | 40.23 | 6.4 | 1.66 | 16.62 | 3.45 | 35.40 | 7.8 | j | H2_lm2_15_17 | w20130827_00226_w | JET_UWISH2_000.31666-0.18594 |
| UWISH2_000.32730+0.20233 | 266.79646 | -28.76171 | 31.46 | 7.5 | 5.76 | 212.38 | 5.04 | 450.39 | 7.8 | u | H2_lm2_15_17 | w20130827_00226_w | PDR_UWISH2_000.31030-0.20300 |
| UWISH2_000.32775+0.21154 | 266.80572 | -28.76610 | 148.28 | 9.8 | 2.91 | 40.24 | 3.48 | 428.10 | 7.8 | u | H2_lm2_15_17 | w20130827_00226_w | PDR_UWISH2_000.31030-0.20300 |
| UWISH2_000.32998+0.20366 | 266.79935 | -28.76011 | 11.38 | 4.1 | 3.27 | 10.70 | 3.60 | 40.00 | 7.8 | u | H2_lm2_15_17 | w20130827_00226_w | PDR_UWISH2_000.31030-0.20300 |
| UWISH2_000.38851+0.62473 | 267.24546 | -28.92752 | 5.23 | 1.8 | 5.41 | 34.87 | 4.31 | 47.96 | 8.6 | j | H2_lm2_15_17 | w20130827_00214_x | JET_UWISH2_000.48489-0.68601 |
| UWISH2_000.39571+0.20634 | 266.43912 | -28.49095 | 17.04 | 3.6 | 6.75 | 26.22 | 5.29 | 121.43 | 6.4 | u | H2_lm2_15_16 | w20130827_00176_y | PDR_UWISH2_000.40129+0.21193 |
| UWISH2_000.39726+0.20853 | 266.43792 | -28.48849 | 64.85 | 8.4 | 6.59 | 5525.55 | 5.30 | 6375.84 | 6.4 | u | H2_lm2_15_16 | w20130827_00176_y | PDR_UWISH2_000.40129+0.21193 |
| UWISH2_000.40382+0.21417 | 266.43633 | -28.47996 | 140.67 | 14.7 | 5.19 | 891.35 | 5.11 | 695.27 | 6.4 | u | H2_lm2_15_16 | w20130827_00176_y | PDR_UWISH2_000.40129+0.21193 |
| UWISH2_000.41135+0.56867 | 267.20401 | -28.87906 | 10.77 | 3.0 | 2.74 | 27.84 | 3.98 | 108.63 | 8.6 | u | H2_lm2_15_17 | w20130827_00214_x | PDR_UWISH2_000.41634-0.56827 |
| UWISH2_000.41656+0.56825 | 267.20666 | -28.87438 | 241.30 | 29.3 | 6.10 | 47.51 | 4.03 | 222.50 | 8.6 | u | H2_lm2_15_17 | w20130827_00214_x | PDR_UWISH2_000.41634-0.56827 |
| UWISH2_000.45198+0.69240 | 267.34905 | -28.90793 | 12.11 | 3.0 | 4.64 | 31.18 | 3.95 | 65.46 | 8.6 | j | H2_lm2_15_17 | w20130827_00214_x | JET_UWISH2_000.48489-0.68601 |
| UWISH2_000.46375+0.69183 | 267.35542 | -28.89754 | 33.83 | 5.4 | 6.02 | 33.35 | 3.58 | 44.08 | 8.6 | j | H2_lm2_15_17 | w20130827_00214_x | JET_UWISH2_000.48489-0.68601 |
| UWISH2_000.47577+0.10395 | 266.78827 | -28.58375 | 315.34 | 15.2 | 6.57 | 11084.29 | 6.76 | 9244.19 | 8.6 | u | H2_lm2_15_17 | w20130827_00214_z | PDR_UWISH2_000.50861-0.09983 |
| UWISH2_000.47915+0.70944 | 267.38171 | -28.89339 | 28.64 | 6.1 | 5.36 | 95.27 | 4.06 | 149.50 | 8.6 | j | H2_lm2_15_17 | w20130827_00214_x | JET_UWISH2_000.48489-0.68601 |
| UWISH2_000.48097+0.70716 | 267.38054 | -28.89665 | 6.87 | 2.5 | 2.98 | 19.91 | 4.53 | 94.59 | 8.6 | j | H2_lm2_15_17 | w20130827_00214_x | JET_UWISH2_000.48489-0.68601 |
| UWISH2_000.48113+0.69815 | 267.37181 | -28.88588 | 65.91 | 7.0 | 4.66 | 130.65 | 5.22 | 327.87 | 8.6 | j | H2_lm2_15_17 | w20130827_00214_x | JET_UWISH2_000.48489-0.68601 |
| UWISH2_000.48123+0.71211 | 267.38555 | -28.89297 | 19.81 | 4.3 | 4.45 | 18.26 | 4.32 | 32.65 | 8.6 | j | H2_lm2_15_17 | w20130827_00214_x | JET_UWISH2_000.48489-0.68601 |
| UWISH2_000.48162+0.70885 | 267.38257 | -28.89096 | 7.34 | 2.7 | 3.55 | 5338.14 | 4.55 | 7995.51 | 8.6 | j | H2_lm2_15_17 | w20130827_00214_x | JET_UWISH2_000.48489-0.68601 |
| UWISH2_000.48347+0.11515 | 266.80372 | -28.58297 | 53.79 | 7.1 | 8.88 | 277.54 | 6.61 | 529.51 | 8.6 | j | H2_lm2_15_17 | w20130827_00214_z | JET_UWISH2_000.48596-0.11519 |
| UWISH2_000.48780+0.11562 | 266.80673 | -28.57951 | 16.90 | 4.1 | 4.86 | 26.27 | 6.68 | 86.61 | 8.6 | j | H2_lm2_15_17 | w20130827_00214_z | JET_UWISH2_000.48596-0.11519 |
| UWISH2_000.48984+0.11501 | 266.80734 | -28.57745 | 26.50 | 5.4 | 4.48 | 193.47 | 5.83 | 836.79 | 8.6 | j | H2_lm2_15_17 | w20130827_00214_z | JET_UWISH2_000.48596-0.11519 |
| UWISH2_000.49102+0.64245 | 267.32307 | -28.84876 | 8.14 | 3.0 | 5.31 | 32.65 | 4.58 | 49.05 | 8.6 | j | H2_lm2_15_17 | w20130827_00214_x | JET_UWISH2_000.48489-0.68601 |
| UWISH2_000.50459+0.78770 | 267.47334 | -28.91176 | 25.07 | 5.6 | 3.80 | 52.54 | 4.61 | 222.02 | 10.9 | u | H2_lm2_15_17 | w20130827_00238_x | PDR_UWISH2_000.57908-0.85893 |
| UWISH2_000.51701+0.65611 | 267.35170 | -28.83350 | 33.30 | 6.2 | 4.54 | 25.22 | 4.60 | | | | | | |